Origin of NMR Spectral Features in MCM-41 at Low Hydrations

by

Mohamad Niknam

A thesis
presented to the University of Waterloo
in fulfillment of the
thesis requirement for the degree of
Master of Science
in
Physics

Waterloo, Ontario, Canada, 2010

I hereby declare that I am the sole author of this thesis. This is a true copy of the thesis, including any required final revisions, as accepted by my examiners.

I understand that my thesis may be made electronically available to the public.

Abstract

Although extensive literature exists on NMR of water in MCM-41, the origin of a number of NMR spectral features in this material had not been understood. Specifically, the OH proton resonance observed in the dry material disappears completely as it is hydrated to 0.2 mono-layer hydration level. The purpose of this study was to gain insight into the physical basics for these spectral features and in the process broaden our understanding of behaviour/interactions of water molecules in porous material. First, measurements of MAS spectra as a function of temperature and hydration, at very low hydrations, made possible a definitive spectral peak assignment. Second, using 1D and 2D selective inversion recovery and magnetization exchange experiments, as well as MAS and non-MAS techniques, magnetization exchange between the water protons and surface OH group protons was quantified. The present results lead to the conclusion that chemical exchange is not responsible for producing the observed changes in proton spectra in MCM-41 as this material is hydrated up to the 0.2 mono-layer hydration level. This represents an important result as it is at odds with what is assumed in the literature in this connection and means that previous conclusions about hydration dynamics in this material need to be revisited. A dynamics model of water interaction with the surface OH hydration sites was introduced to explain the observed proton spectra. The model can successfully predict the observed chemical shifts and temperature dependent changes of proton spectra in the very low hydration MCM-41.

Acknowledgements

I am very thankful to my supervisor, Dr. Hartwig Peemoeller, whose encouragement, enthusiasm, guidance and support from the initial to the final stages of this project enabled me to develop an understanding of the subject. I appreciate his time and effort which guided me through this research as well as the valuable feedback on this thesis. Many thanks goes to Dr. Claude Lemaire. He is a real scientist and I always gained lots of insight with working when him.

It is an honour for me to thank Dr. David Cory for his instructive suggestions and comments.

I would like to thank Firas Mansour who has helped me in making MCM-41 sample and advised me in teaching. I am indebted to many of my colleagues who have supported me; especially Jianzhen Liang, who has initiated simulation programs. I would like to thank Dr. Jamal Hassan and Colin Guthrie who have provided me with MCM-41 samples. I appreciate the helps from the science machine shop and science electronic shop.

I could not be here without getting help and encouragement from Dr. Nader Ghahramany, Shiraz University, Dr. Alexandre Nikitenko, Imperial College London and Dr. John Ellis from Theory Division, CERN.

I also would like to thank my family in Iran who are always supportive. My special thanks go to my wife, Negar Ghahramani, for being best part of my life with her unconditional love and endless support.

To my Love

Negar

Contents

List of Tables

List of Figures

Chapter 1

Introduction

Mesoporous MCM-41, a member of the silica molecular sieve family, has attracted considerable interest over the last 10-15 years. Because of its large specific surface area, well defined geometry and relative ease of synthesis, MCM-41 promises to find application as an effective host for catalytic materials, molecular sieves, medical phantoms and carriers for drug delivery. Study of water in MCM-41 is important because in various applications the pore volume is filled with an aqueous medium; e.g.water containing halogenated hydrocarbons and H_2 in palladized MCM-41 for ground water re-mediation schemes. Therefore in order to design and control systems involving nano-porous materials and water, having knowledge about hydration processes, hydration sites and water-surface interactions, is crucial. In addition, the well defined pore shape of MCM-41 (hexagonal pore channels of uniform diameter) make this material an attractive model system for water molecule dynamics, water phases and water-surface interactions in confined geometries.

Nuclear magnetic Resonance (NMR) has made significant contributions to studies of porous materials and dynamics of their hydration. Bronnimann et al. [1] studied dehy-

dration of the silica gel surface and identified three proton resonance lines. They assigned a narrow peak at a chemical shift position of 3 ppm (proton resonance frequency shift, expressed in parts per million, due to specific electronic environment) to water molecules, a broad peak to hydrogen bonded (HB) OH groups and a narrow peak at 1.7 ppm to single (S) OH groups. They also found that magnetization exchange occurs between HB OH groups and S OH groups by spin diffusion. Another study on water and silica gel, done by Overloop et al. [2], concluded that the magnetization exchange rate between surface water protons and silanol group protons is on the order of 10 s^{-1}, while it is of the order of 100 s^{-1} between free water protons and surface water protons. Magnetization exchange between spin groups can mask the intrinsic NMR relaxation and spectral parameters so that only apparent parameters are observed. Then, detailed knowledge about the exchange is needed in order to determine the intrinsic parameters.

Zhao et al.[3] reported the existence of three kinds of OH groups on the surface of MCM-41: HB OH, S OH and germinal OH groups. They also studied the effect of dehydroxylation on these groups. Hwang et al. [4, 5] constructed an exchange model for hydrated MCM-41 with three water spin groups: slow, fastI and fastII. The slow water group resides on the surface and is connected to the fastI group. The fastII group is only connected to the fastI group. Pizzanelli et al. reported [6] that in fully hydrated MCM-41, all surface OH groups are accessible to water molecules. They also estimated the average distance between HB OH group protons as 2.9 Åand that between single OH group protons as 4.3 Å. They observed magnetization exchange between HB OH group protons and single OH group protons, mediated by water molecules. Grunberg et al. [7] measured NMR spectra in MCM-41 for different hydration levels. Their sample only contained single OH groups and water. They concluded that fast exchange occurs between water protons and single OH

protons. Trebosc et al. [8] found a broad resonance line between 2 to 8 ppm chemical shift position and associated it with surface water. They used 2D exchange analysis to show that this broad line exchanges magnetization with the OH peak on the 10 ms time scale. Using deuterium NMR a definitive assignment of water proton and deuteron resonances to water at single and hydrogen bonded surface hydroxyl groups in MCM-41 was reported by Hassan et al. [9]

Although extensive research already has been done on water molecule behaviour in MCM-41, controversy still exists on details of hydration dynamics. For example, the details of coordination of water on surface groups, or hydration sites, are not completely known. Residence time of water molecules on hydration sites and various motional time scales of water are not well understood. Additional complexity is added to this problem if one asks what these parameters are at different hydrations and temperatures. Diffusion rates of water molecule in porous materials have been explored only to a limited extent and need to be addressed as a function of hydration level. Another important question in this field deals with the details of pore filling processes. Because water molecules in confined geometries can form different number of bonds, of various strengths, to surface hydration sites and to other water molecules, unusual phases of water may exist. For example water will not freeze in MCM-41 even at temperatures lower than 0 °C. Different phases of water in confined geometries need to be studied in more detail. Finally, magnetization exchange processes between water spins and surface spin groups are not well understood and could lead to false interpretation of NMR spectra.

In order to study these questions, we explore behaviour of water molecules inside pores of MCM-41 and their interactions with the surface hydration sites, with particular emphasis on the role played by magnetization exchange processes in producing the observed

resonance lines as well as the changes in their shape with hydration and temperature.

Chapter two briefly describes NMR basic theory. The various experimental methods in sample preparation and performing NMR experiments are presented in chapter three. Chapter four explores the difference between dry proton signal and hydrated proton signal of MCM-41 sample and discusses possibility of the observed differences being produced by chemical exchange between water protons and surface OH protons. Chapter five details studies of very low hydration MCM-41 samples and dynamics of water molecules on hydration sites.

Chapter 2

Basics of NMR

Nuclear Magnetic Resonance (NMR) is a form of radio frequency spectroscopy in the frequencies range $\nu_0 = 5 - 1000$ MHz, which is based on the interaction between magnetic nuclei and a magnetic field. Consider magnetic nuclei, or nuclear spins, placed in an external field B_0 in the z-direction. Because of this magnetic field, nuclear spin will precess around the z-axis with Larmor frequency $\boldsymbol{\omega_0} = \gamma \mathbf{B_0}$, where γ is the gyromagnetic ratio. Zeeman interaction will produce a nuclear spin energy level hierarchy or scheme and at thermal equilibrium the energy level populations will satisfy Boltzmann statistics. As a consequence an equilibrium magnetization M_0 will be set up along the z-direction. Nuclear spins can absorb energy from an rf field of frequency ν_0 if their magnetic energy levels are separated by $h\nu_0$, where h is Planck's constant.

Typically the rf field B_1 is applied in the xy-plane and changes the thermal equilibrium population distribution, and therefore M_z, and magnetization components M_x and M_y can results. The evolutions of spin magnetization components are described by a set of differential equations known as the Bloch equations: [13]

$$\begin{aligned}
\frac{dM_x}{dt} &= \gamma(M_y B_0 + M_z B_1 \sin(\omega t)) - \frac{M_x}{T_2} \\
\frac{dM_y}{dt} &= \gamma(M_z B_1 \cos(\omega t) - M_x B_0) - \frac{M_y}{T_2} \\
\frac{dM_z}{dt} &= -\gamma(M_x B_1 \sin(\omega t) + M_y B_1 \cos(\omega t)) + \frac{M_0 - M_z}{T_1}
\end{aligned} \tag{2.1}$$

The spin-lattice relaxation time T_1 is the characteristic time for recovery of M_z to its equilibrium value M_0. In contrast with T_1 processes, which involve energy absorption by the lattice from the spin system in order to recover the equilibrium state population distribution, T_2 processes, or spin-spin relaxation processes, produce phase changes in the precession of nuclear spins. Consider total magnetization vector M_0 along the z-axis. Let a B_1 field change this magnetization vector by 90 degrees and bring it into the xy-plane. Because spins are experiencing slightly different magnetic fields due to presence of neighbouring spins, they will precess at slightly different Larmor frequencies, which will cause dephasing of the net magnetization in xy-plane. The time constant which describes the decay of the total magnetization vector in the xy-plane is called the spin-spin relaxation time, T_2 . The decaying induction signal in the coil surrounding the sample is called the Free Induction Decay (FID) and can be used to find T_2 of the sample.

2.1 Spin Interaction Hamiltonian

The total Hamiltonian for nuclear spins in NMR consist of an external and an internal part. The external part contains Zeeman splitting due to B_0 and also the spin interaction with the applied rf field B_1. The internal Hamiltonian contain various terms of which

the dipole-dipole term and chemical shift term are of particular interest in the present discussion. [10] The various elements of the Hamiltonian are summarized in equation 2.2.

$$\begin{aligned} \mathcal{H} &= \mathcal{H}_{ext} + \mathcal{H}_{int} \\ \mathcal{H}_{ext} &= \mathcal{H}_z + \mathcal{H}_{rf} \\ \mathcal{H}_{int} &= \mathcal{H}_{cs} + \mathcal{H}_D \end{aligned} \tag{2.2}$$

2.1.1 External Hamiltonian

The Zeeman interaction is the largest term and other interactions are perturbations to this main term. The Zeeman term arises from the interaction of nuclear spin (I) with external field B_0 :

$$\mathcal{H}_z = -\gamma\hbar\mathbf{I}\cdot\mathbf{B_0} \tag{2.3}$$

where γ is the gyromagnetic ratio. The allowed magnetic energy then would be

$$E_z = -\gamma\hbar B_0 m_I \ldots\ldots\ldots (m_I = I, I-1..., -I) \tag{2.4}$$

Using (2.4) in the Boltzman distribution gives the population ratio between energy levels

$$\frac{N_{m_I-1}}{N_{m_I}} = \exp(\frac{-\gamma\hbar B_0}{kT}) \tag{2.5}$$

where k is the Boltzmann constant and T is the absolute temperature. Although the population difference between lower energy state and higher energy state is not large compared to the total number of spins in the sample, this small deviation from zero is very important since it is the only part that contributes to the NMR signal.

The form of the Hamiltonian for the interaction of spins with the applied magnetic field B_1 is the same as that of the Zeeman Hamiltonian:

$$\mathcal{H}_{rf} = -\gamma\hbar\mathbf{I}\cdot\mathbf{B_1} \tag{2.6}$$

Although various time durations and amplitudes of the B_1 field are used in NMR to manipulate the spins, most commonly used B_1 fields are in the form of $\frac{\pi}{2}$ and π pulses. Consider the net magnetization vector along the z-axis. A $\frac{\pi}{2}$ pulse will turn the magnetization vector into the xy-plane while a π pulse will invert it to the -z direction, which means that there is no magnetization in the xy-plane. This would be a good way to define a π pulse; to apply a pulse of different lengths and determine the length for which the pulse does not produce any signal. The same pulse with half the pulse length would be a $\frac{\pi}{2}$ pulse.

After B_1 is switched off , the spins dephase (T_2 process) and redistribute to Zeeman energy levels and magnetization returns to the equilibrium state (T_1 process). The response from the spins during these processes is normally recorded via the NMR signal. [11]

2.1.2 Internal Hamiltonian

Nuclear spins see the effect of the main B_0 field directly through the Zeeman Hamiltonian and indirectly through the chemical shift Hamiltonian. Chemical shift results from

the effect of electronic environment on nuclear spins. The mechanism of chemical shift involves the induction of a current in the molecular electron cloud by the main B_0 field, which produces a magnetic field at the site of the nucleus. This induced field, to a good approximation, is linearly dependent on main magnetic field B_0.

$$\mathbf{B_{induced}} = \delta \mathbf{B_0} \tag{2.7}$$

where δ is called the chemical shift and is usually indicated in parts per million (ppm) and is defined as:

$$\delta(ppm) = \frac{\omega - \omega_0}{\omega_0} \tag{2.8}$$

where ω is the Larmor frequency of the nuclei in the molecular site of interest and ω_0 is the reference Larmor frequency of that nuclei in same magnetic field. Then the chemical shift Hamiltonian can be written [12]

$$\mathcal{H}_{cs} = -\gamma \hbar \mathbf{I} \cdot \mathbf{B_{induced}} \tag{2.9}$$

The Hamiltonian for dipole-dipole interactions for a system of N spins has the form [13]

$$\mathcal{H}_D = \frac{1}{2} \sum_{j=1}^{N} \sum_{k=1}^{N} [\frac{\mu_\mathbf{j} \cdot \mu_\mathbf{k}}{r_{jk}^3} - \frac{3(\mu_\mathbf{j} \cdot \mathbf{r_{jk}})(\mu_\mathbf{k} \cdot \mathbf{r_{jk}})}{r_{jk}^5}] \tag{2.10}$$

where $\mu_\mathbf{j}$ and $\mu_\mathbf{k}$ are magnetic moment vectors for spin j and k, respectively, and $\mathbf{r_{jk}}$ is the position vector between them. For the interaction between two spins, 1 and 2, equation 2.10 can be written: [13]

$$\mathcal{H}_D = \frac{\gamma_1\gamma_2\hbar^2}{r^3}(A+B+C+D+E+F) \tag{2.11}$$

where

$$\begin{aligned}
A &= I_{1z}I_{2z}(1-3\cos^2\theta) \\
B &= -\frac{1}{4}(I_1^+I_2^- + I_1^-I_2^+)(1-3\cos^2\theta) \\
C &= -\frac{3}{2}(I_1^+I_{2z} + I_{1z}I_2^+)\sin\theta\cos\theta e^{-i\phi} \\
D &= -\frac{3}{2}(I_1^-I_{2z} + I_{1z}I_2^-)\sin\theta\cos\theta e^{i\phi} \\
E &= -\frac{3}{4}I_1^+I_2^+\sin^2\theta e^{-2i\phi} \\
F &= -\frac{3}{4}I_1^-I_2^-\sin^2\theta e^{2i\phi}
\end{aligned}$$

and θ is the angle between r_{jk} and B_0, while $\frac{\gamma_1\gamma_2\hbar^2}{r^3}$ is the dipolar interaction coupling constant. This constant is 10^4 times weaker than the Zeeman coupling constant, which supports the idea of adding dipolar coupling as a perturbation to the Zeeman energy levels. Consider two identical spins in B_0, which will results in four Zeeman energy levels (two are degenerate). Term A is diagonal and only connects each state to itself. Term B is off-diagonal and energy conserving that connects two degenerate levels together. Terms C,D,E and F produce admixtures between levels, which produces second order energy shifts. In many instances T_2 effects are dominated by terms A and B and the truncated Hamiltonian $\mathcal{H}_D^0 = A + B$ is used in related discussions.

2.2 Magic Angle Spinning (MAS)

MAS can reduce effects of dipolar broadening in solid samples and narrow the resonance line drastically. Consider the angular dependency of $\mathbf{r_{jk}}$ in terms A and B. If the sample mechanically rotates around an axis which makes angle θ' to the main field, as shown in Figure 2.1, the term $(1 - 3\cos^2\theta_{jk})$ in the dipolar Hamiltonian should be replaced by an average value. For fast rotation this average value can be shown to be [13]

$$< 1 - 3\cos^2\theta_{jk} >_{avg} = (1 - 3\cos^2\theta')\frac{3\cos^2\gamma_{jk} - 1}{2} \tag{2.12}$$

If the sample rotates at $\theta' = 54.7°$, the magic angle, the first term of the right hand side would go to zero, which will remove the effect of dipole-dipole interaction. To accomplish this, the sample is placed into a Zirconia rotor with a fan-shape cap and mechanical rotation is produced by blowing gas through the rotor cap.

2.3 Exchange Analysis

Different spin groups in a sample can exchange magnetization. Exchange of magnetization by magnetic interaction between spins A and B is called magnetic exchange. In contrast, when proton spins are exchanged between A and B by breaking chemical bonds of the hydrogen atom involved, the exchange of magnetization is due to chemical exchange between the two different spin groups. Study of magnetization exchange can be an important part of the elucidation of intrinsic spin space parameters and their evolution.

Consider a simple model of a two spin-group system, as indicated in Figure 2.2.

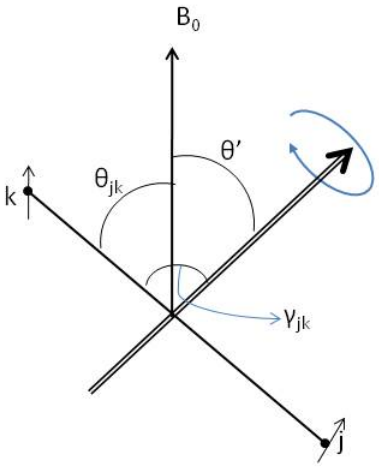

Figure 2.1: Angles that have been used to describe the effect of rotation on dipole-dipole interaction between spins j and k.

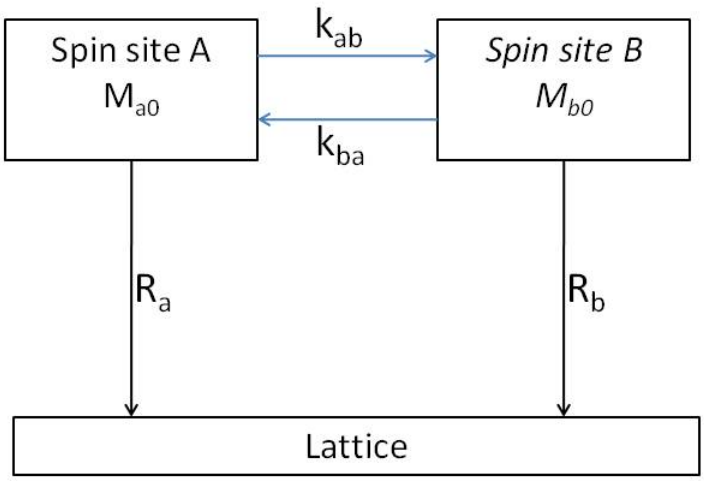

Figure 2.2: Schematic representation of a sample containing two different spin groups A and B, which exchange magnetization.

R is the intrinsic rate of loosing energy to the lattice, the spin-lattice relaxation rate and k_{ab} is the rate of magnetization exchange from site A to site B. Therefore, the evolution of the magnetization of the spin groups can be written as

$$\begin{aligned} \frac{dM_a}{dt} &= (-R_a - k_{ab})M_a + k_{ba}M_b \\ \frac{dM_b}{dt} &= (-R_b - k_{ba})M_b + k_{ab}M_a \end{aligned} \tag{2.13}$$

These equations can be expressed in matrix form

$$\frac{d}{dt}\begin{pmatrix} M_a \\ M_b \end{pmatrix} = \begin{pmatrix} R_{11} & R_{12} \\ R_{21} & R_{22} \end{pmatrix} \begin{pmatrix} M_{a0} \\ M_{b0} \end{pmatrix} \tag{2.14}$$

where

$$\begin{aligned} R_{11} &= -R_a - k_{ab} \\ R_{12} &= k_{ba} \\ R_{21} &= k_{ab} \\ R_{22} &= -R_b - k_{ba} \end{aligned}$$

When finding eigenvalues and eigenvectors for this eigenvalue problem, a unitary transform matrix would be found which diagonalizes matrix R:

$$\begin{aligned} \lambda_{\pm} &= \frac{(R_{11}+R_{22}) \pm \sqrt{(R_{11}-R_{22})^2+4R_{12}R_{21}}}{2} \\ \mathbf{U} &= \begin{pmatrix} 1 & b \\ a & 1 \end{pmatrix} \text{ and } \mathbf{U^{-1}} = \frac{1}{1-ab}\begin{pmatrix} 1 & -b \\ -a & 1 \end{pmatrix} \end{aligned} \tag{2.15}$$

where

$$\begin{aligned} a &= \frac{\lambda_+ - R_{11}}{R_{12}} \\ b &= \frac{\lambda_- - R_{22}}{R_{21}} \end{aligned}$$

The final answer then becomes

$$\frac{d}{dt}\begin{pmatrix} M_a \\ M_b \end{pmatrix} = \frac{1}{1-ab}\begin{pmatrix} e^{\lambda_+ t} - abe^{\lambda_- t} & b(e^{\lambda_- t} - e^{\lambda_+ t}) \\ a(e^{\lambda_+ t} - e^{\lambda_- t}) & e^{\lambda_- t} - abe^{\lambda_+ t} \end{pmatrix}\begin{pmatrix} M_{a0} \\ M_{b0} \end{pmatrix} \tag{2.16}$$

Equation (2.16) gives the evolution of magnetization for each site of a two spin-group system.

For more than two spin groups, the problem can be solved using the same method. First, the rate matrix R should be diagonalized

$$\mathbf{U^{-1}RU} = \lambda \tag{2.17}$$

and then the general answer would be of the form

$$\mathbf{M} = \mathbf{M_0 U} \exp(\lambda \mathbf{t}) \mathbf{U^{-1}} \tag{2.18}$$

Therefore, the measured magnetization components for a two spin-group system can be written as [14]

$$M_i(t) = C_i^- e^{-\lambda_- t} + C_i^+ e^{-\lambda_+ t} \tag{2.19}$$

where

$$\begin{aligned} C_a^+ &= \frac{M_{a0} - M_{b0} b}{1 - ab} \\ C_a^- &= \frac{(M_{b0} - M_{a0} a) b}{1 - ab} \end{aligned} \tag{2.20}$$

In these exchange experiments, the M_0 's are initial magnetizations of each spin group. $\lambda^{\pm}$ are the apparent relaxation rates and $C_i^{\pm}$ are the apparent magnetization fractions, which can be obtained from the experimental data.

Figure 2.3 shows a simulation for a 2D time domain exchange experiment. The surface contains sets of FID curves recorded along the time, t, axis for different τ spacings [for a description of the inversion recovery experiment look at section 3.3.2]. Here τ is also the time that spin groups can exchange magnetization. Consider a recovery curve for a particular value of t, Figure 2.4 This recovery curve contains two exponential components that can be resolved by fitting the data to a two-exponential function. The time constant of the fast exponential, λ_+^{-1}, is the time constant of the fast decaying exponential curve at the top of this recovery curve and λ_-^{-1} is the time constant for the lower exponential curve.

Curves with constant τ are FIDs. If one extrapolates all of the slow exponential T_1-

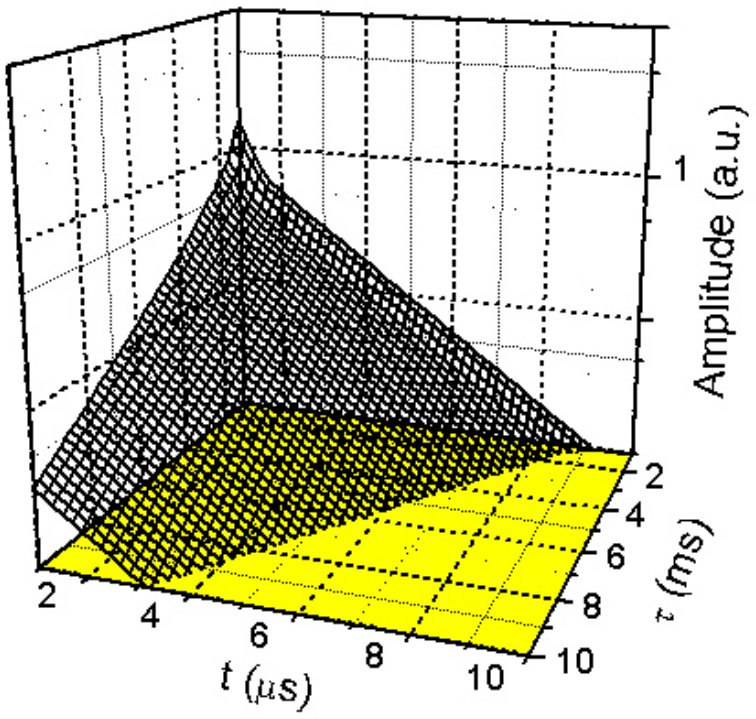

Figure 2.3: Typical result of a 2D time domain magnetization recovery experiment. Figure with permission from author [15]. The abbreviation a.u.denotes arbitrary units.

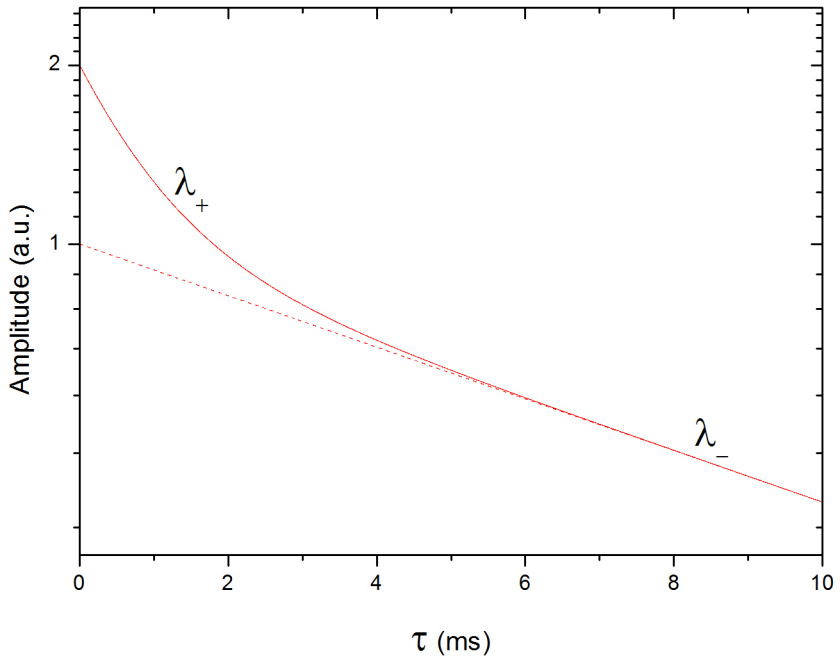

Figure 2.4: A recovery curve which has two components with different T_1 time constants.

component amplitudes to the $\tau = 0$ plane, another FID curve is produced, which is the FID of the slow-recovering magnetization component and which is called a reconstructed FID. Similarly, projecting all of the fast exponential T_1-component amplitudes to the $\tau = 0$ plane, produces the reconstructed FID for the fast T_1-component. Fitting Gaussian and exponential decay terms to these reconstructed FIDs, yields the different $C^{\pm}$ fractions.

Inserting these fractions into equation 2.20 and using initial magnetizations and apparent time constants, the intrinsic exchange rates k_{ab}, k_{ba} and the intrinsic relaxation rates can be found. These calculations were performed with software existing in the NMR laboratory called EXFIT. [16]

Combining exchange analysis with selective inversion techniques, or soft-hard (SH) T_1

experiments, leads to better resolved apparent magnetization components and therefore to an improved analysis. Consider a system which has a solid-like spin group and a liquid-like spin group. Assume that the T_2 of the solid-like proton group is very short, of the order of 10 μ s, and the T_2 of the liquid-like proton group is much longer, of the order of milliseconds. A low amplitude, long (longer than 100 μ s) π pulse will invert the liquid-like spins but will not have a significant effect on solid-like spins. This type of pulse is called a soft pulse and the experiment is called a soft-hard T_1 inversion recovery experiment.

Chapter 3

Experimental

3.1 Sample preparation

MCM-41 was prepared using the synthesis method in [17, 18]. Fumed silica powder with 99.8% purity (metal free) and particle size 0.07 μm was obtained from SIGMA. Tetramethyl ammonium hydroxide (TMAOH, 97% pure) was also obtained from SIGMA and Cetyltrimethyl ammonium bromide (CTABR, 99%) was obtained from ALDRICH. First TMAOH and CTABR were dissolved in distilled, deionized water by stirring at 500 rpm and 30 °C. When a clear solution was obtained, silica powder was added and the solution stirred for three hours. 200 g of water was used to make up the solution. The final molar composition was: 1.0 SiO_2 , 0.19 TMAOH, 0.27 CTABR, 40 H_2O. After ageing the sample for 24 hours it was placed in an autoclave and heated to 125 °C for 68 hours. The resulting white solution contains MCM-41 which was washed and filtered. It was then calcined at 700 °C for 8 hours in order to remove organic templates.

Figure 3.1 shows an electron micrograph of MCM-41 showing highly ordered hexagonal

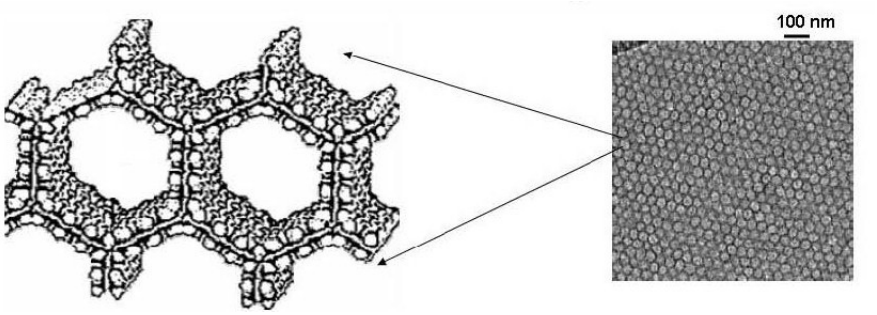

Figure 3.1: High resolution transmission electron micrograph of MCM-41 cross section and a model of the hexagonal pores, from [11].

pores. The pore size distribution and specific surface area can be determined using nitrogen adsorption-desorption measurements. Confirmation of the highly ordered nature of the prepared MCM-41 comes from X Ray Diffraction (XRD) experiment.

In the present study, MCM-41 synthesized by Dr. J. Hassan with pore diameter of 36 Å, was used. This MCM-41 has surface area to mass ratio of 980 m^2/g. The sample's characteristics have been determined with nitrogen absorption-desorption and XRD experiments under the same condition as in [17, 11] and essentially identical results were obtained as reported in these references.

Complete hydroxylation was achieved by saturating MCM-41 with water. It may be noted that to fully saturate the pores the MCM-41 in water was pumped several times in order to remove air from the pores. The saturated sample was allowed to stand for two days. After allowing the MCM-41 to air-dry, it was dried under 10^{-3} Torr vacuum at 80 °C to remove all water.

The hydration level is conveniently specified through n, the number of water molecules per OH groups. Three categories of samples were prepared; dry MCM-41, "low hydration" MCM-41 with n=1 and "very low hydration" MCM-41 with n<0.5 . Specific sample

hydration details are elaborated upon in chapters 4 and 5, which deal with NMR results for low hydration MCM-41 and very low hydration MCM-41, respectively.

3.2 NMR aparatus

Time domain experiments were performed using a home build, pulsed NMR spectrometer operating at a proton Larmor frequency of 30 MHz. The NMR probe uses a free standing, gold coated solenoidal coil. For each experiment 1 cm of sample was placed in a 7 mm od thin-walled NMR sample tube from Wilmad LabGlass Company, and flame sealed to maintain the desired initial conditions. Temperature control was achieved with a Micromega CN 77000 unit which controls the flow of hot gas for temperatures above room temperature and flow of cold nitrogen gas, from a liquid nitrogen dewar, for temperatures below room temperature.

Frequency domain experiments were carried out with a Bruker 11.7 Tesla ultra shield magnet and a Bruker DMX500 spectrometer. A Bruker MAS probe with a 4 mm Zirconia rotor and rotor cap with O-ring from Wilmad LabGlass Company were used. A Bruker BVT3000 temperature controller maintained sample temperature at the set value in the range of -130 to 80 °C by controlling the flow of N_2 gas passing through a liquid nitrogen dewar for low temperature experiments and flow of hot N_2 gas for high temperature experiments.

3.3 NMR mesurements

3.3.1 Free Induction Decay (FID)

The FID signals were recorded after applying a 90° pulse. The pulse sequence is

$$-90^{\circ}_{x} - t_{Acq} \tag{3.1}$$

In the 500 MHz spectrometer, the FID was typically Fourier transformed to the frequency domain. Chemical shift calibration was done using a 4,4-dimethyl-4-silapentane-1-sulfonic acid (DSS) sample.

3.3.2 Spin-lattice relaxation time (T_1) measurement

To measure T_1 the inversion recovery method was used. The pulse sequence for this experiment is

$$-180^{\circ}_{x} - \tau - 90^{\circ}_{x} - t_{Acq} - t_{rep} \tag{3.2}$$

The length of 180° pulse in the 30 MHz spectrometer for a hard-hard pulse sequence was 3.4 μs whereas for the soft-hard experiment the 180° pulse length was 200 μs. 40 τ values were chosen to cover the recovery process. The time t is the data acquisition time and t_{rep} is the repetition time, which was chosen to be at least $5T_1$ to prevent saturation of component magnetizations.

3.3.3 2D exchange measurement

2D exchange experiments were performed using the three-pulse sequence

$$-90^{\circ}_{x} - t_1 - 90^{\circ}_{x} - t_m - 90^{\circ}_{x} - t_{Acq} - t_{rep} \tag{3.3}$$

The first 90 ° pulse is a preparation pulse which brings magnetization components to the xy-plane. During encoding time t_1, different spin groups gain different phases based on their specific Larmor frequency. With the second 90 ° pulse, the magnetizations for each spin group will be projected along the z-axis. The time t_m is the mixing time, which allows transfer of Zeeman magnetization between different spin groups. The third 90 ° pulse is the detection pulse. For a particular 2D measurement, t_m was kept fixed while t_1 steps were automatically adjusted. The number of points for the FID along t_{Acq} was 1000. It may be noted that t_{Acq} is also commonly denoted by t_2. By choosing different mixing times t_m, the exchange time scale can be studied.

Chapter 4

Low Hydration MCM-41 (n=1)

In this chapter, experiments on MCM-41 samples with n = 1 hydration level are presented and discussed. Adding water molecules to a dry MCM-41 sample produces large changes in spectral features of the proton resonance line observed in the dry sample. These changes have been studied using time domain and frequency domain NMR experiments.

4.1 Problem statement

A typical $^1H\ MAS$ spectrum for fully hydroxylated, dry MCM-41 is shown in Figure 4.1. This spectrum is a Fourier transform of the free induction decay signal acquired at 500 MHz. Two main peaks are observable in this spectrum. To decompose the spectrum into components, Lorentzian lines were fitted to the data using a least squares fitting procedure. The Lorentzian lines are of the form

$$y(\nu) = y0 + (\frac{2A}{\pi})\frac{w}{4(\nu - \nu_c)^2 + w^2} \tag{4.1}$$

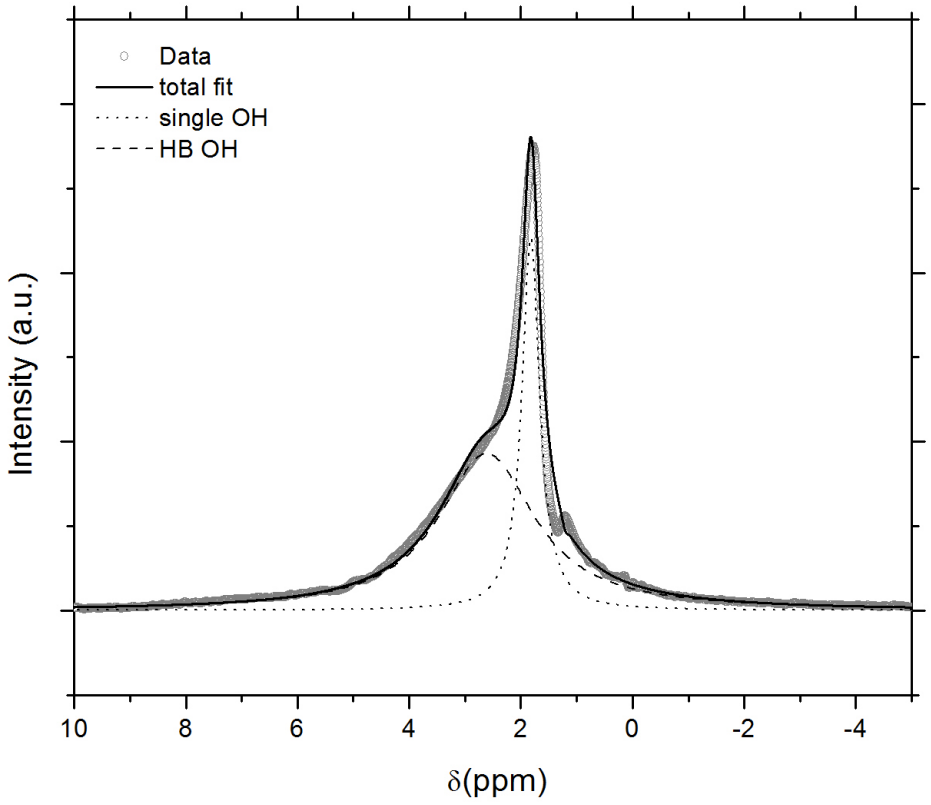

Figure 4.1: ^1H *MAS* spectrum for dry, fully hydroxylated MCM-41, at room temperature and 10 kHz spinning rate. Two Lorentzian lines are fitted to the data; a narrow peak at (1.82±0.05) ppm with width of (0.38±0.03) ppm and a broader peak at (2.61±0.05) ppm with width of (2.09±0.03) ppm.

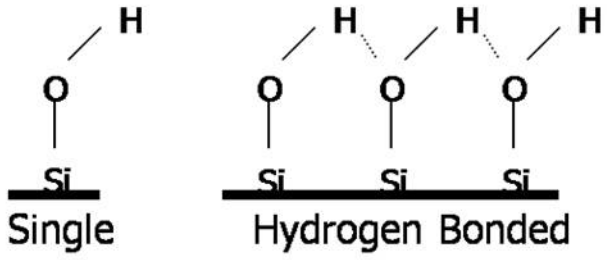

Figure 4.2: Two possible hydration sites on MCM-41 pore surface

where A is the area under the line, ν_c is the center frequency of Lorentzian line and w is the width of the line at half maximum. The fit gives a sharp peak centred at 1.8 ppm and a broad peak, with less height, centred at 2.6 ppm. The present spectrum is consistent with the spectrum in dry MCM-41 reported in [15].

There are two kinds of hydration sites on internal surfaces of MCM-41 nano tubes. Figure 4.2 shows a simplified schematic of these OH group configurations. [3],[9] It has been shown that heating the sample to 673 K (400 °C) will decrease the number of hydrogen bonded OH groups. [3] In this process water molecules are formed leaving pairs of Si atoms connected to one oxygen and also some single OH groups. After 24 hours of heating, all of HB OH groups vanish and only isolated OH groups remain on the surface. This kind of sample "400dry sample" has been used for assignment of the decomposed peaks in the normal dry sample. [15] Figure 4.3 shows a $^1H\ MAS$ spectrum of the 400dry sample. Only the sharp peak at 1.8 ppm remains, which implies that the sharp Lorentzian line in dry MC-41 corresponds to single OH group proton resonances and the broad line is due to HB OH groups.

Figure 4.4 shows $^1H\ MAS$ spectra for the fully hydroxylated MCM-41 sample, with hydration level n = 1, recorded at two different temperatures. This hydration corresponds

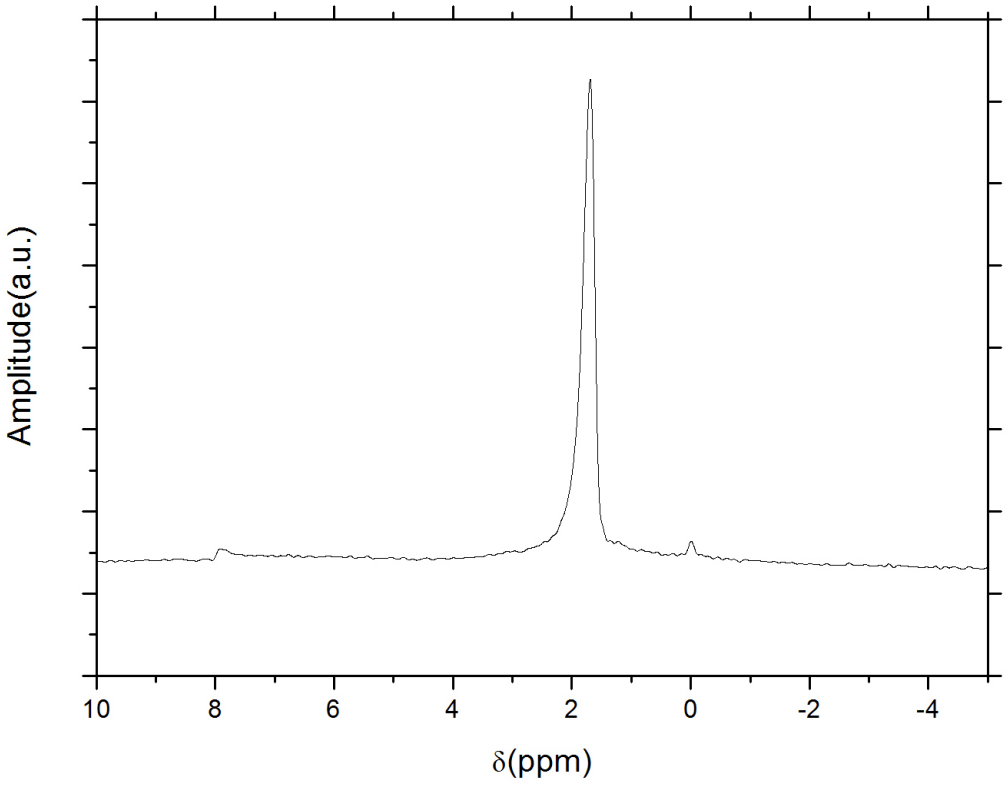

Figure 4.3: ^1H *MAS* spectrum of 400dry sample at room temperature and 10 kHz spinning rate. The peak has a width of (0.22±0.03) ppm and position of (1.71±0.05) ppm.

to one water molecule per surface OH group and is also known as 0.2 mono-layer hydration. This spectrum is in agreement with the spectrum in a 0.2 mono-layer hydration MCM-41 sample given in [15]. Consider the spectrum for T = 270 K. The single OH group peak seen at 1.8 ppm in the dry sample, Figure 4.1, has disappeared completely from this spectral position in the hydrated sample. In addition, all, or at least a significant part of the peak associated with hydrogen bonded OH group protons is no longer separately observable in the hydrated sample. Instead a relatively narrow peak, representing 60% of the magnetization, has appeared at 3.4 ppm and a smaller, much broader peak, representing 40% of magnetization at about 6.1 ppm. Assignment of these resonances is not straight forward and requires further investigation.

4.2 Results and Discussion

In bulk water, at room temperature, the proton resonance is centred at about 4.8 ppm. However, at the present hydration level bulk water formation is not expected and single water molecule hydration is expected to dominate (some dimer and possibly trimer formation may also occur). Figure 4.5 indicates chemical shifts (given as superscripts in ppm) expected for the protons involved. [7]

It would appear reasonable to suppose that the appearance of the main peak in the hydrated sample, located at 3.4 ppm, and the disappearance of the OH group resonance is a consequence of chemical exchange between the water and surface hydroxyl hydrogens at a rate that is fast compared with the frequency difference between the resonances. Although such exchange could explain the disappearance of the 1.8 ppm OH resonance (and part of the OH resonance centred at 2.6 ppm) it cannot explain the appearance of the broad peak

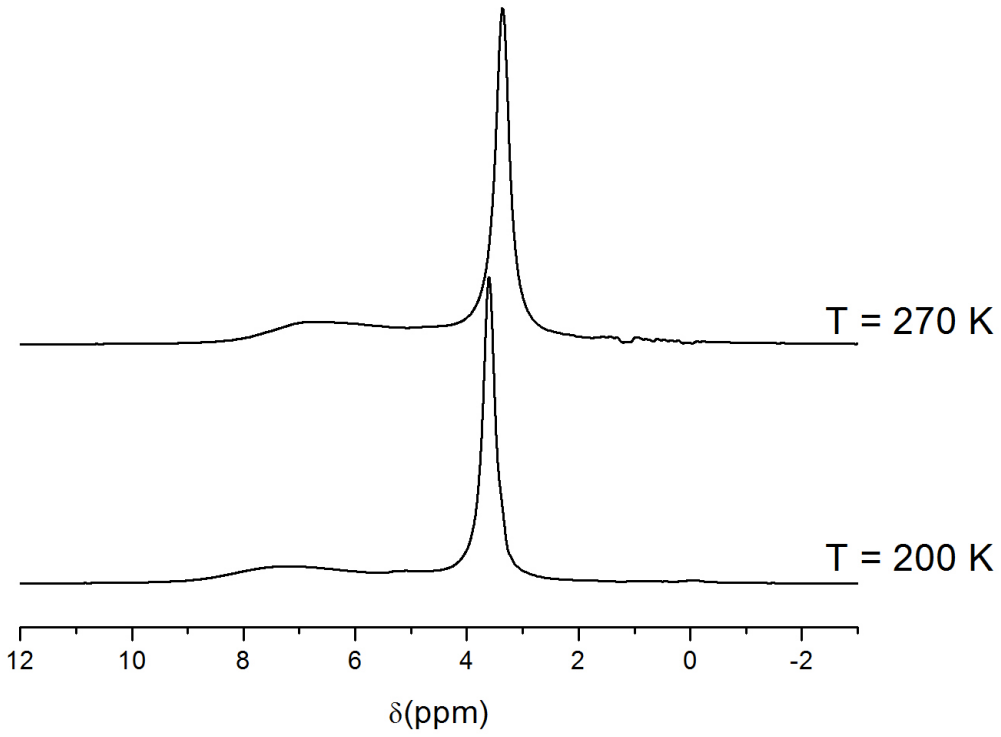

Figure 4.4: ^1H MAS spectra of fully hydroxylated MCM-41 with hydration level n = 1, at 10 kHz spinning rate recorded at 270 K and 200 K .

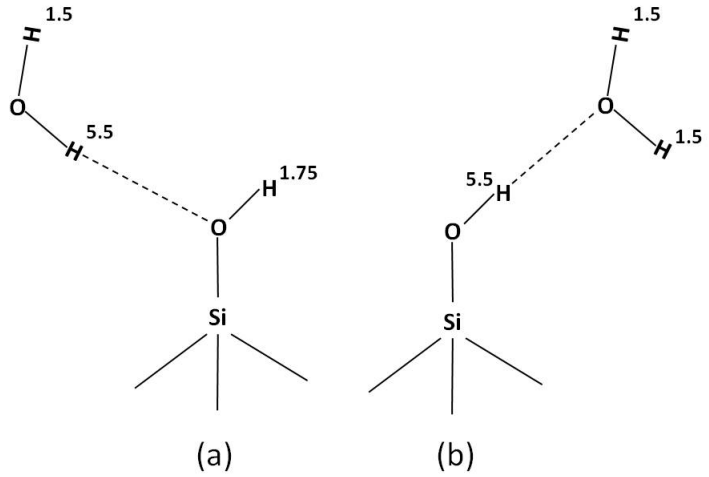

Figure 4.5: Geometric configuration of interaction of water molecules with surface OH groups. Superscripts indicate expected proton chemical shifts in ppm.

at 6.1 ppm.

To gain additional insight into the role played by chemical exchange in controlling the observed spectrum in the n = 1 sample, a first step is to obtain an estimate of the actual exchange rate required for the surface OH resonances and water resonance to coalesce. From the stoichiometry of the hydrated sample and the spectral decomposition of the dry sample, see Figure 4.1, it is ascertained that the magnitude of the water signal, magnitude of hydrogen bonded OH group signal and magnitude of single OH group signal are proportional as 66:13:21. For purposes of arriving at an estimate of the required exchange rate we consider a 3-site model consisting of water protons, single OH group protons and hydrogen bonded OH group protons. We approximate the water proton signal by a Lorentzian line, at 3.5 ppm, contributing 66% to the total signal. Considering the areas under the two spectral lines in Figure 4.4 it is evident that most of the intensity of the narrow line is

associated with water protons. We take this line width of 145 Hz as a rough estimate of the width of the simulated Lorentzian line for water protons. The surface OH group proton signals are simulated using the line characteristics from Figure 4.1. Therefore, single OH group proton and hydrogen-bonded OH group proton signals have been simulated as Lorentzian lines at 1.8 ppm and 2.6 ppm with magnitudes of 21% and 13% and widths of 190 Hz and 1045 Hz, respectively.

Figure 4.6 shows a series of simulated spectral lines for this 3-site model for different chemical exchange rates between surface protons and water protons. In this approximate model we have assumed that no exchange occurs between the single OH and HB OH sites and they both have the same exchange rate to water protons.

This exchange simulation shows that the exchange rate needed for the proton resonances of solid OH groups and water to coalesce is definitely more than 1000 s^{-1}.

A number of water hydrogen-surface hydrogen exchange rates are available in the literature for related systems. For example, an exchange rate of about 1000 s^{-1} was reported for hydrated zeolite at room temperature. [19] An exchange rate of 1000 s^{-1} is estimated from the data presented in [20] for a wood keratin sample with approximately the same hydration level as for the MCM-41 sample with n = 1. To date this rate of chemical exchange in partially hydrated MCM-41 has not been reported upon.

An indication that chemical exchange may not be the main mechanism causing the disappearing of the OH peaks upon hydration, comes from the temperature dependence of the MAS spectrum for the n = 1 sample. Chemical exchange is a thermally activated process so that if the chemical exchange rate in the present case were indeed 1000 s^{-1} at room temperature, then one would expect the reappearance, or at least partial reappearance, of the initial OH peaks at the 1.8 ppm and 2.6 ppm position as the temperatures is lowered.

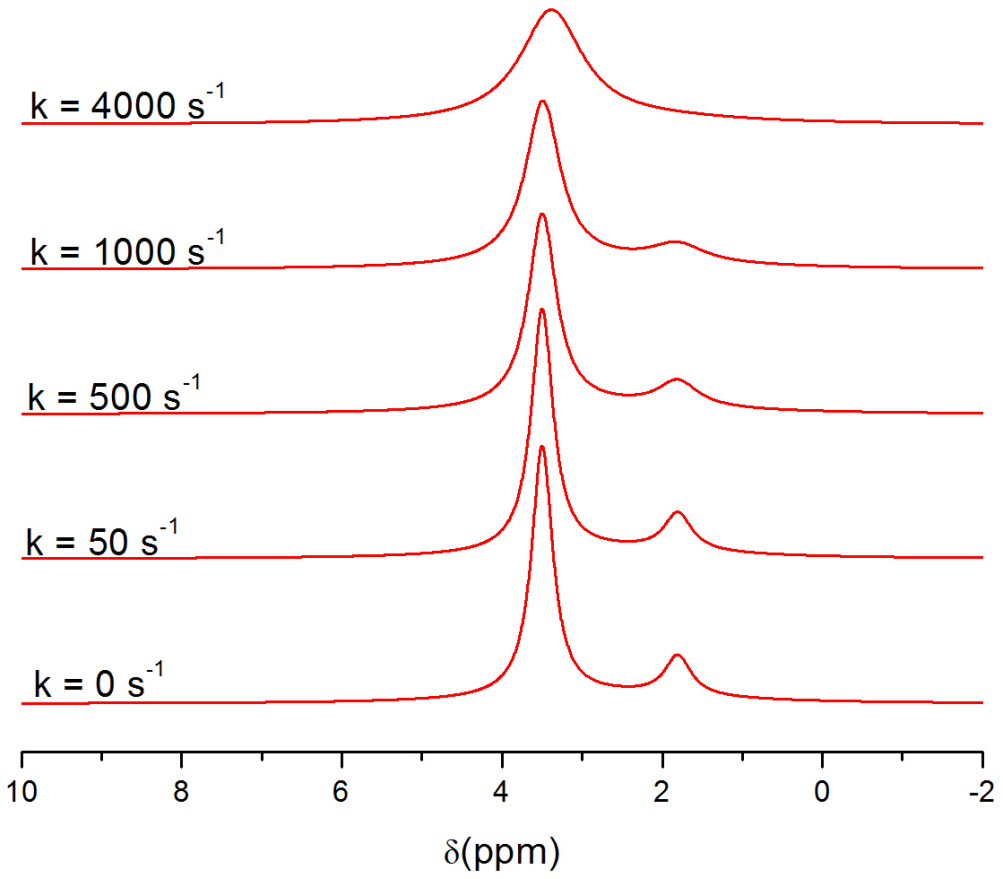

Figure 4.6: Simulation of Lorentzian lines for three site model (S-OH, HB-OH and W), showing an estimate of exchange rate, k, required to produce coalescence of the two main peaks of surface hydroxyl groups and water. Here k is the magnetization exchange rate from HB-OH and S-OH group protons to water protons.

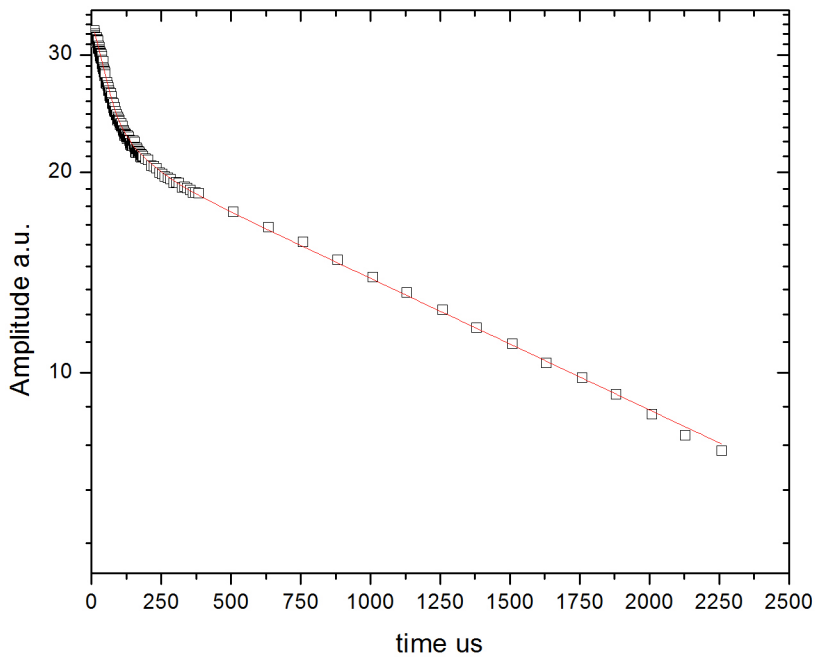

Figure 4.7: FID signal of MCM-41 sample with n = 1, taken at room temperature and Larmor frequency of 30 MHz. The solid line was calculated from equation (4.2) using the best fit parameters obtained from a least square fit:

Spin Group	T_2	Amplitude
Gaussian	$(51 \pm 4)\mu s$	(12.6±1.0) %
Exponential 1	$(94 \pm 5)\mu s$	(22.1±1.3)%
Exponential 2	(2.2±0.1) ms	(65.3±1.4)%

However, as can be seen from Figure 4.4 there is no indication of the reappearance of OH peaks, or of any other major changes in the spectral lines, as the sample temperature is lowered to 200 K.

The loss of resolution with respect to the water and OH proton resonances in MCM-41 MAS experiments, is partially recovered in a static time domain experiment.This is the

consequence of the very different T_2 values of water and surface OH protons. Figure 4.7 shows a Free Induction Decay (FID) signal for hydrated MCM-41 sample, with n = 1, acquired at a Larmor frequency of 30 MHz.

This FID signal is well represented by the sum of two exponential components and a Gaussian:

$$S_{(t)} = A_g \exp((-\ln 2)\frac{t^2}{(T_{2g})^2}) + A_1 \exp\frac{-t}{T_{21}} + A_2 \exp\frac{-t}{T_{22}} \tag{4.2}$$

Equation (4.2) was fitted to the FID data using a least-squares approach and the solid line in Figure 4.7 was calculated from this equation using the best-fit parameters given in the figure caption.

Assignment of different components was achieved by comparing the FID signal of fully hydroxylated sample to that of 400dry sample. Doing so, the Gaussian component, with $T_2^{HB-OH} = 51\ \mu s$, was assigned to protons of the hydrogen bonded OH groups and the exponential component M_{S-OH}, with $T_2^{S-OH} = 94\ \mu s$, corresponds to protons of single surface OH groups. The remaining component with $T_2^w = 2.2\ ms$ can be assigned to water molecule protons. The fact that three expected signals (from single and hydrogen bonded OH group protons and water protons) are resolved in the FID experiment, combined with the order of magnitude difference between T_2 relaxation times of surface OH group protons and water protons, is expected to allow us to gain additional insight into magnetization exchange in this sample from 2D time domain recovery experiments. In particular, the use of selective excitation, using soft pulses, is expected to be very useful in this connection. [21]

At 293 K the recovery curve in the $T_1 Hard - Hard$ ($T_1 HH$) experiment in MCM-41

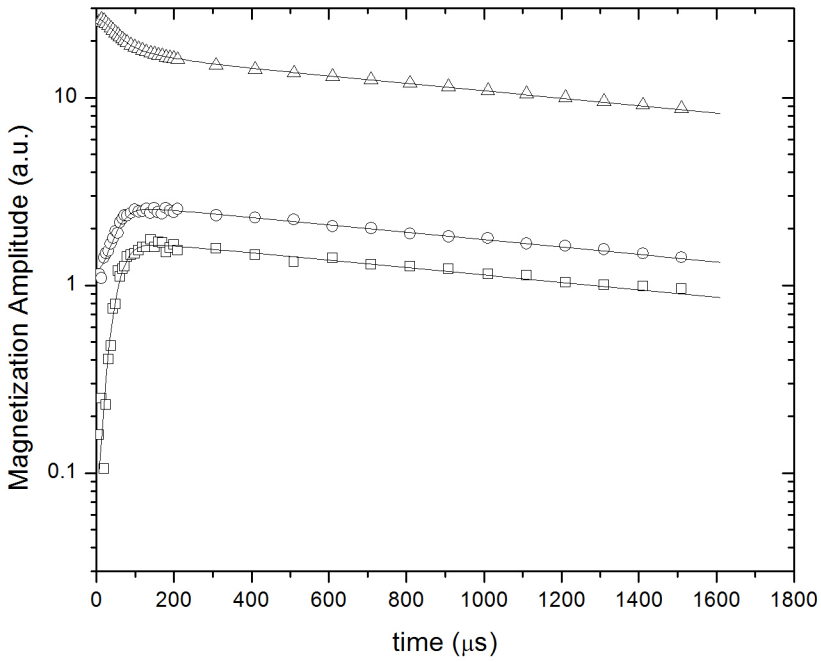

Figure 4.8: Reconstructed FIDs for Soft-Hard inversion recovery experimental data at room temperature. Squares give the reconstructed FID for the component with fastest $T_1 = (2.3 \pm 0.3)$ ms, circles for the component with $T_1 = (12.7 \pm 0.9)$ ms and triangles for the slowest component with $T_1 = (134 \pm 4)$ ms. Equation (4.2) was fitted to each of these curves and the best-fit parameters are given in Table 4.1

with n = 1 is exponential, indicating that exchange between spin groups is in, or at least near, the fast exchange regime on the T_1 time scales of the three groups. The reconstructed FIDs, obtained from 2D time domain analysis for the T_1 Soft-Hard (T_1SH) experiment, are plotted in Figure 4.8. The fact that negative FIDs are observed for magnetizations with T_1^+ and T_1^0 is a further indication of the presence of magnetization exchange in this system. [22]

Table 4.1: Intrinsic and apparent T_1 relaxation parameters obtained from 2D time domain recovery experiments at 20 °C.

	Intrinsic T_1 [15]	Apparent T_1 fractions (%)		
Spin groups	T_1	$\lambda^+ = 2.3\ ms$	$\lambda^0 = 12.7\ ms$	$\lambda^- = 134\ ms$
HB OH protons	(1.5±0.3) s	-5.7±0.7	-5.0± 0.7	16.7± 0.7
Single OH protons	(6.0±0.5) s	-0.4± 0.9	-0.24± 0.9	17.8± 0.9
Water protons	(86±9) ms	6.4± 0.2	9.8± 0.2	60.9± 0.2

Each reconstructed FID was fitted to (4.2) with the best-fit magnetization fractions denoted by $C_{S-OH}^{+,0,-}, C_{HB-OH}^{+,0,-}$ and $C_W^{+,0,-}$. The best-fit parameters obtained from this analysis, as well as the T_1 time constants are summarized in Table 4.1.

As derived below, these magnetization fractions and time constants are essential for a meaningful magnetization exchange analysis for this system.

The observation of three distinct T_1 components in the SH inversion recovery experiment, taken together with the identification of single OH, hydrogen bonded OH and water proton signals in the FID signal, prompts us to consider a 3-site exchange model. Defining the reduced magnetization for the i^{th} component as

$$m^i(\tau) = \frac{M_0^i - M_z^i(\tau)}{2M_0^i} \tag{4.3}$$

the evolution of this component's magnetization is governed by

$$\frac{dm^i(\tau)}{d\tau} = -(R_i + K_{ij} + K_{ik})m^i(\tau) + K_{ji}m^j + K_{ki}m^k \tag{4.4}$$

where R_i is the spin-lattice relaxation rate and K_{ij} is magnetization exchange rate from

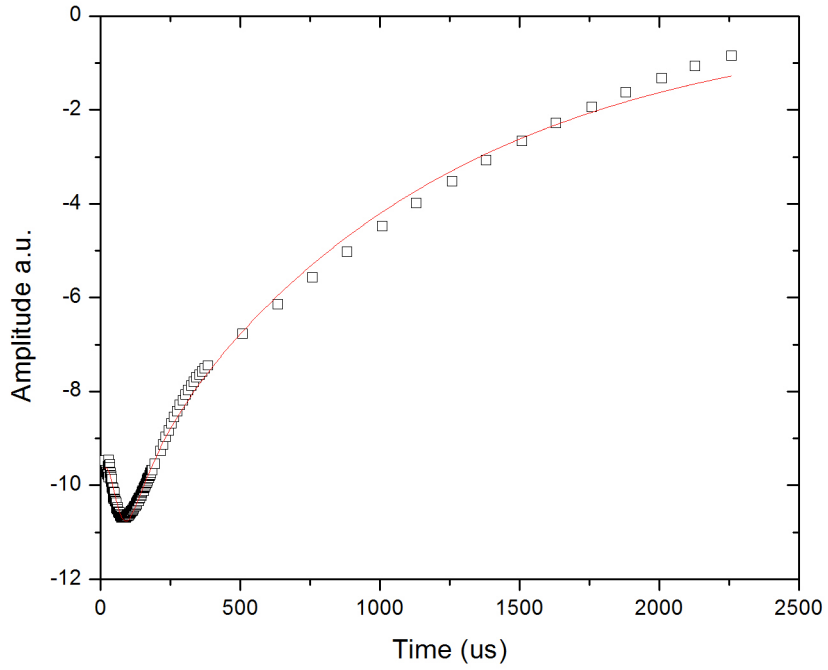

Figure 4.9: FID signal, following hard 90 ° pulse applied immediately after a Soft inversion pulse. From this we obtain inverted fractions: $M^{S-OH} = (72.3 \pm 9.7)\%, M^{HB-OH} = (32.1 \pm 5.5)\%$ and $M^{W} = (90.0 \pm 6.0)\%$.

site i to j. The parameters i, j and k are cyclic and we can assign i:HB-OH, j:S-OH and k:W. In the SH inversion recovery experiment, the goal is to selectively invert particular spins and leave others untouched. To know the fraction of the magnetization of each spin group that was initially inverted, the values of the Zeeman magnetization M_0^i immediately following the soft pulse, are needed. These initial magnetizations have been calculated by fitting equation (4.2) to the FID signals following a 90° hard pulse applied immediately after the soft pulse (i.e. $\tau = 10\ \mu s$) , Figure 4.9.

With the initial magnetizations, the data given in Table 4.1 , and intrinsic spin group

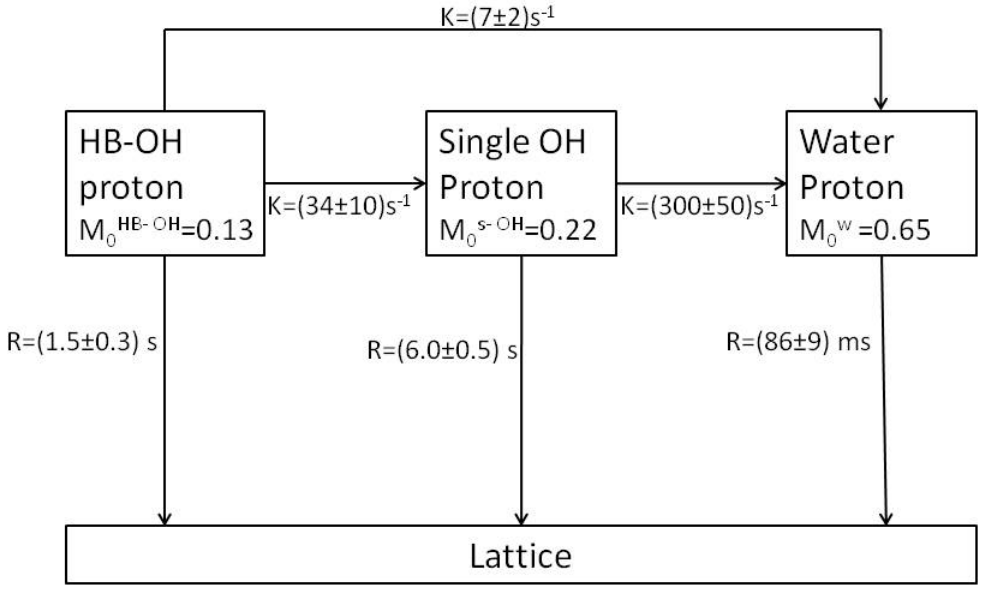

Figure 4.10: Three-site exchange model. Exchange rates and intrinsic T_1 relaxation rates for each site are shown beside the arrows.

sizes from FID experiment, Figure 4.7, the set of coupled differential equations (4.4) were solved for all component magnetization parameters using the EXFIT program. For more details pertaining to the exchange analysis see Section 2.3 and [14] . Figure 4.10 shows the resulting three-site exchange model and indicates calculated intrinsic exchange rates and spin-lattice relaxation rates.

4.3 Conclusion

Exchange simulations show that in order to produce effective changes in spectral line position and shapes for resonance lines located at 2 ppm and 5 ppm, exchange rates higher than 1000 s^{-1} are needed. The T_1SH experiment and associated exchange analysis indicates that the largest exchange rate occurs between single OH protons and water protons, with $k_{SOH-w} = 300\ s^{-1}$. This strongly suggests that chemical exchange between surface OH group protons and water protons is not fast enough to cause the observed spectral line changes as dry MCM-41 is hydrated.

The averaging of chemical shift positions, due to the dynamics of water molecule on the surface of MCM-41, could be responsible for the observed spectral line changes and is investigated in the next chapter.

Chapter 5

Very Low Hydration MCM-41(n<0.5)

As discussed in the previous chapter, adding water molecules to dry MCM-41 modifies surface OH group resonances, in a way that leaves them unresolved from water proton resonances. At $n = 1$ hydration level, at which we have performed our first experiments, there is one water molecule per surface OH group, which corresponds to two times more signal from water protons than from surface OH group protons. In order to better resolve spectral features of surface OH group protons, before these resonance lines completely disappear underneath the water proton resonance line, measurement at lower hydration levels is expected to help. Heating the dry sample to 400 °C also removes HB-OH groups, leaving only single surface OH group proton resonances, Figure 4.3, which reduces the complexity of the spectrum. [9]

Table 5.1: Very low hydration sample characteristics

sample name	exposure time (min)	total increase in signal	moisture content(n)	δ_{OH} (ppm)	δ_{hydOH} (ppm)	δ_W (ppm)
M5min	5 min	$(18 \pm 6)\%$	0.09 ± 0.02	1.82 ± 0.05	2.10 ± 0.05	2.9 ± 0.1
M10min	10 min	$(27 \pm 6)\%$	0.13 ± 0.02	1.83 ± 0.05	2.23 ± 0.05	3.2 ± 0.1
M20min	20 min	$(69 \pm 7)\%$	0.34 ± 0.02	1.82 ± 0.05	2.23 ± 0.05	3.0 ± 0.1
M30min	30 min	$(76 \pm 8)\%$	0.38 ± 0.02	1.91 ± 0.05	2.36 ± 0.05	2.8 ± 0.1

5.1 Sample preparation and characteristics

To prepare very low hydration samples, fully hydroxylated MCM-41 was kept at 400 °C for 24 hours. The dried sample was transferred to a glove box, which was continuously flushed with dry nitrogen gas, and then placed into a zirconia rotor which was sealed with an o-ring fitted cap. After acquiring the MAS spectrum of surface OH group protons of the dry sample at 500 MHz with 10 kHz spinning rate, the sample was exposed to water vapour in a desiccator. With increasing exposure time, different hydration levels were achieved. Table 5.1 shows these sample characteristics.

Following each hydration step the sample was sealed again to maintain its moisture content during the experiment. At the end of each experiment the sample was re-dried under vacuum, at 80 °C, to monitor any potential changes in dry signal. No change in signal relative to that before hydration was observed ensuring that no HB-OH group had formed. In order to monitor possible unwanted changes of hydration, the sample was weighted, using a balance with 10 μg precision, at all steps. It was observed that adding water, up to $n = 0.5$, did not produce any HB-OH groups that remained after re-drying the sample. This suggests that to produce HB-OH groups a specific aqueous environment is needed and as long as hydration was not increased past this level, this sample remained

in the single OH group state.

5.2 Results and Discussions

Figure 5.1 shows modification of dry MCM-41 surface OH group proton resonance (sharp peak-dotted lines) with addition of water to the sample (solid lines).

Areas under these peaks correspond to total magnetization of the sample which is directly proportional to the number of protons in the sample. In order to find total area and other spectral parameters, Lorentzian lines were fitted to the experimental spectrum. For dry MCM-41, one Lorentzian line provided a good fit for the proton resonance peak. For hydrated samples three Lorentzian lines were needed in order to obtain a good fit with the least-square method. The total area was calculated by adding the areas under the three Lorentzian lines. The differences between total magnetization in the dry sample and hydrated samples are indicated in Table 5.1. As already mentioned, each water molecule produces two times the magnetization of a surface OH group. Therefore, in the M5min sample, 18 % increase in total signal means that the number of water molecules equals 9 % of the number of surface OH groups. Figure 5.1 shows that this number of water molecules has modified more than 50 % of dry surface OH proton resonance. An important question is how such a small number of water molecules is able to modify such a large part of the surface OH group proton resonance. The same question applies as we increase the hydration level in the sample.

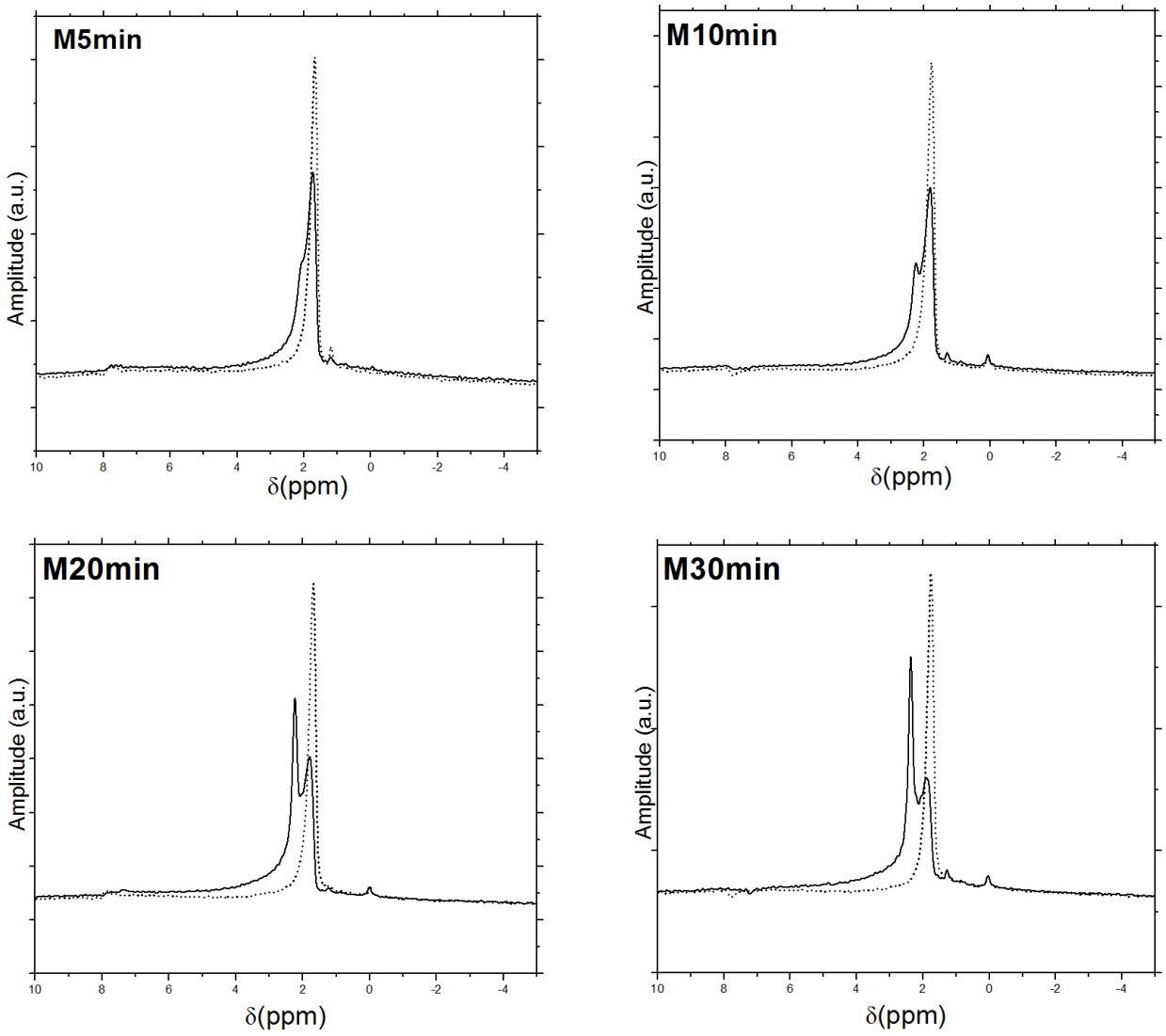

Figure 5.1: Effect of hydration on the dry MCM-41 ^1HMAS spectral line shape at 20 °C. The dotted lines give the dry MCM-41 spectrum and the solid lines give the hydrated MCM-41 spectrum.

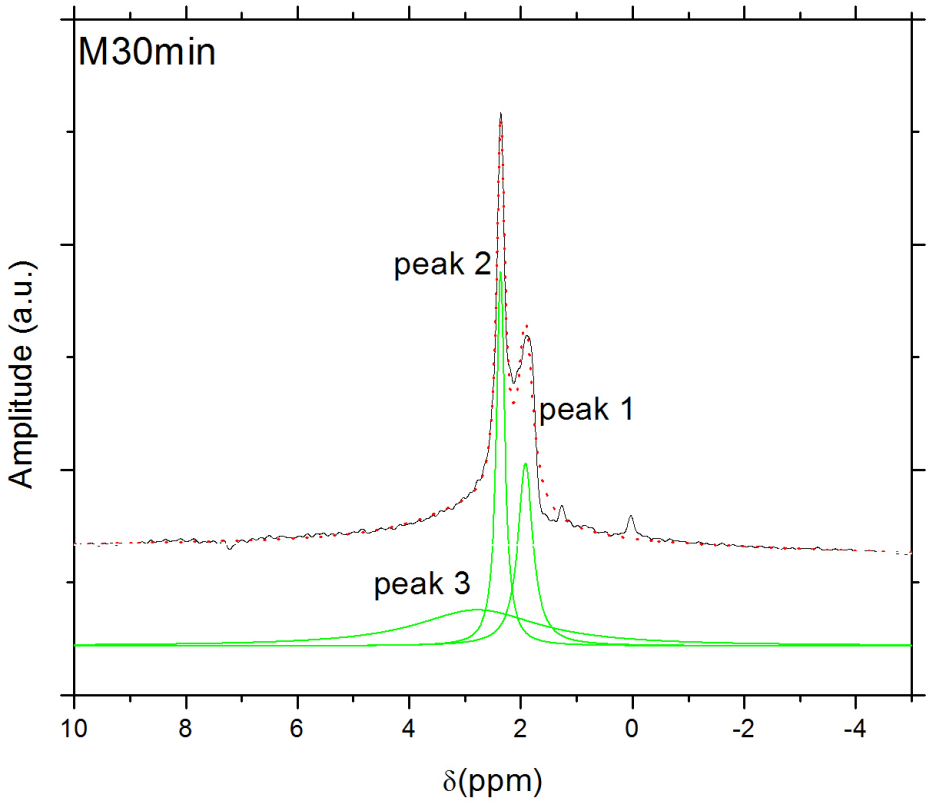

Figure 5.2: Decomposition of a typical ^1HMAS spectrum in the M30min sample at 20 °C into three Lorentzian lines. The solid black line gives data points, red dotted line gives the total fitted curve and green lines are individual Lorentzian lines.

5.2.1 Assignment of peaks

Because a few water molecules can modify a large part of the surface OH proton resonance, it is necessary to perform very low hydration experiments in order to properly track changes in spectral shape of OH proton resonances.

Figure 5.2 shows a typical spectrum for the M30min sample. As mentioned before,

a combination of three Lorentzian lines provides a good fit for the spectrum in hydrated MCM-41, and such a decomposition is also shown in Figure 5.2. First component is a Lorentzian line at a chemical shift position of (1.92±0.05) ppm and with line width of (0.32±0.03) ppm. These parameters are the same for the surface OH resonance in a dry sample. Second component is another narrow Lorentzian line at (2.36±0.05) ppm . Third component is a broad Lorentzian line at a chemical shift position of (2.77±0.05) ppm and with line width of (2.70±0.03) ppm. As hydration level increases, the first narrow peak at 1.92 ppm decreases in amplitude, while the second narrow peak at 2.36 ppm grows. Increasing the hydration level, increases the amplitude of the broad peak. In all hydration experiments at room temperature, the area under the broad peak is equal to magnetization difference between hydrated and the dry sample. These observations prompt us to propose the following assignment for decomposed spectral lines in hydrated samples:

1. The broad peak corresponds to water proton resonance.

2. The narrow peak at 1.92 ppm corresponds to surface OH group proton resonance.

3. The origin of the middle narrow peak at 2.36 ppm is not known and needs to be investigated further. As the reason for a part of OH group proton resonance to shift is likely connected with hydration of OH groups, we call this peak, Hydrated OH peak.

5.2.2 Origin of the hydrated OH peak

As discussed in chapter 4, for the sample with $n = 1$ the spectral line shape does not change appreciably in the temperature range 200 K to 270 K, Figure 4.4. In order to gain additional

insight into the origin of the hydrated OH peak, experiments at different temperatures were also performed in the M20min sample, Figure 5.3. The change of the spectra with temperature is clearly visible and shows that there must be some temperature mediated interaction or process which makes the changes in line shape of ^1HMAS spectrum visible at low hydration. Using a lower hydration sample and a less complex OH group surface system has enabled us to access definitions of peaks and their evolution with temperature in more detail than for the higher hydration samples.

Although exchange of magnetization between water protons and OH protons has been given as a mechanism for some of the observed changes in spectral features as MCM-41 is hydrated [7], we propose that in MCM-41, at this hydration level, exchange of magnetization between water protons and the OH group protons can not produce the observed hydrated OH peak. The reason is that fast exchange between two spin groups can cause their proton resonance lines to coalesce but would not be able to to produce a third resonance line between them. There is also some evidence that chemical exchange between different spin groups in the hydrated MCM-41 sample is not fast enough to induce appreciable spectral changes.

The first supporting evidence of this is that at the higher hydration level of n = 1, as discussed in the previous chapter, the rate of magnetization exchange between water protons and single OH group protons is 300 s^{-1} (see Figure 4.10). However, the exchange rate needed for the water proton resonance to coalesce with OH group resonances in this samples is more than 1000 s^{-1}, which is much larger than the observed exchange rate (see Section 4.2). Such magnetization exchange is expected to be slower still at lower hydrations and therefore cannot be responsible for any observed coalescence.

An excellent experiment that can provide information about magnetization exchange

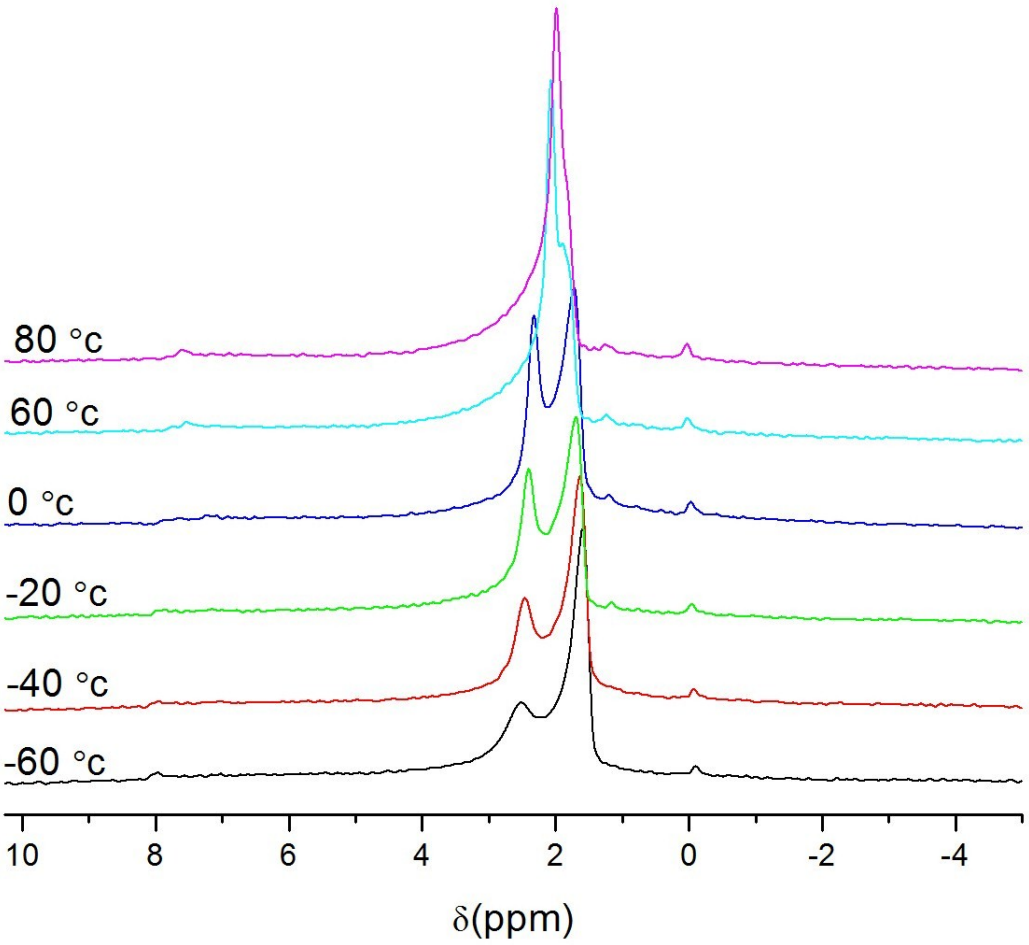

Figure 5.3: Effect of temperature on ^1HMAS signal in M20min sample.

between different spin groups, is a spectrally selective inversion recovery experiment, Figure 5.4 (also see Section 3.3.2). After selectively inverting the magnetizations, if there is no magnetization exchange on the T_1 time scale, the single exponential magnetization recovery of each spin group will be observed. If fast magnetization exchange occurs, each spin group will exhibit more than one recovery time constant in the selective recovery experiment and the resulting multi-exponential recovery curve will have recovery time constants that are common to all other spin groups.

Figure 5.5 shows the recovery curves of magnetization components in the M5min sample at 80 °C. Each of the three recovery curves was obtained by monitoring the recovery of each of the three peaks. Although this is a preliminarily experiment and needs to be repeated to get better signal to noise ratio (e.g. note scatter at short times for the recovery curve defined by triangles), better peak definition and proper T_1 definition by using repetition times longer than 5 times T_1, a study of these magnetization recovery curves can still provide insight. Magnetization recovery time constants for water protons, single OH group protons and hydrated OH protons are given in the caption of Figure 5.5. Three separate curves are indicative of a 3-site exchange scenario. The fastest component in the magnetization recovery curve of hydrated OH protons has the time constant of $(\lambda^+)^{-1} = 19$ ms, which indicates that the highest possible exchange rate between water protons and hydrated OH protons is less than 53 s^{-1}, which is again slow on the T_1 time scale.

Magnetization exchange between different spin groups can also be effectively studied using 2D exchange spectroscopy. Figure 5.6 gives 2D exchange spectra for the M20min sample for a number of mixing times.

At $\tau_M = 1$ ms in the upper-right part of the spectrum, OH peaks are distinguishable. The width of these peaks are expected to have contributions from a small amount of

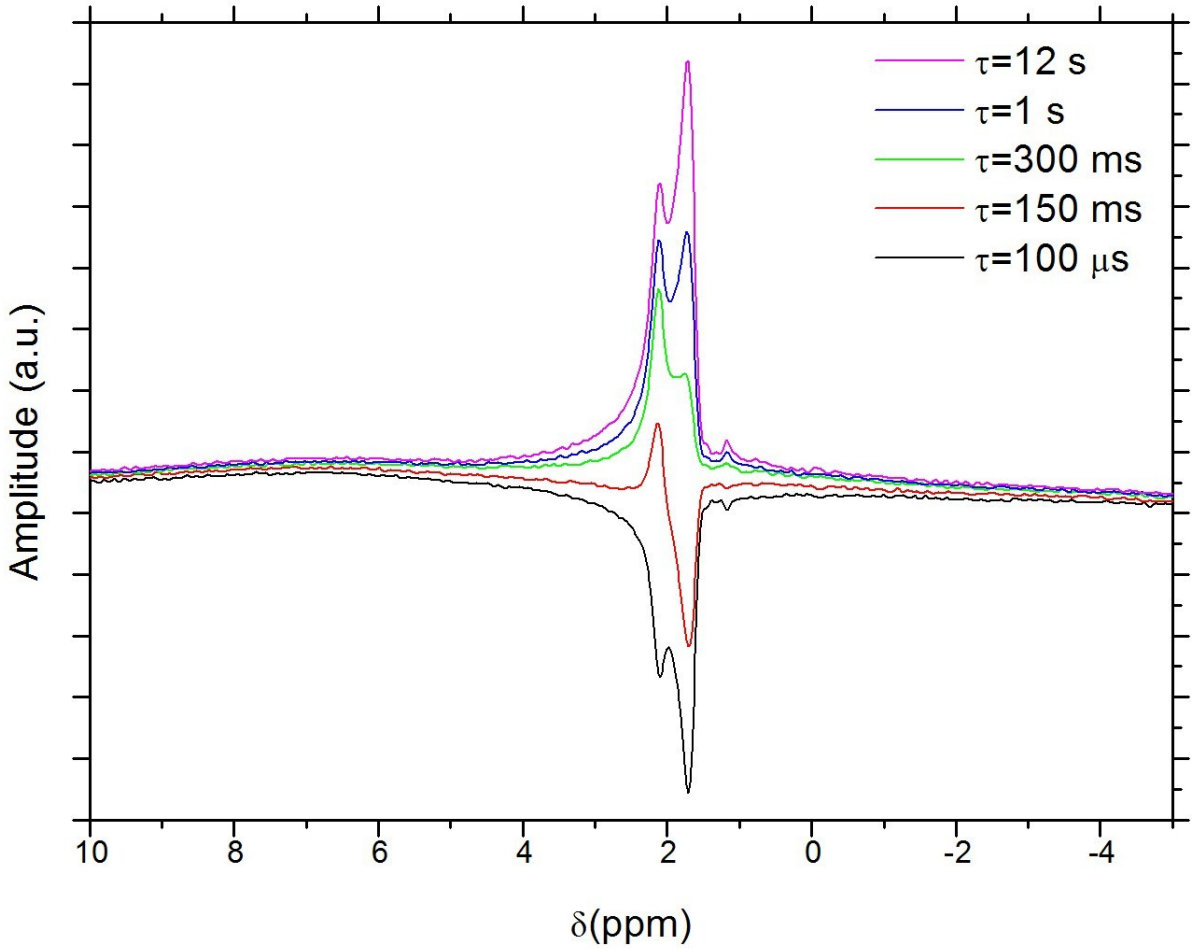

Figure 5.4: Spectrally selective inversion recovery experiment in M5min sample at 20 °C which shows different time constants of magnetization recovery for OH group protons and hydrated OH group protons. A repetition time of 2 s was used.

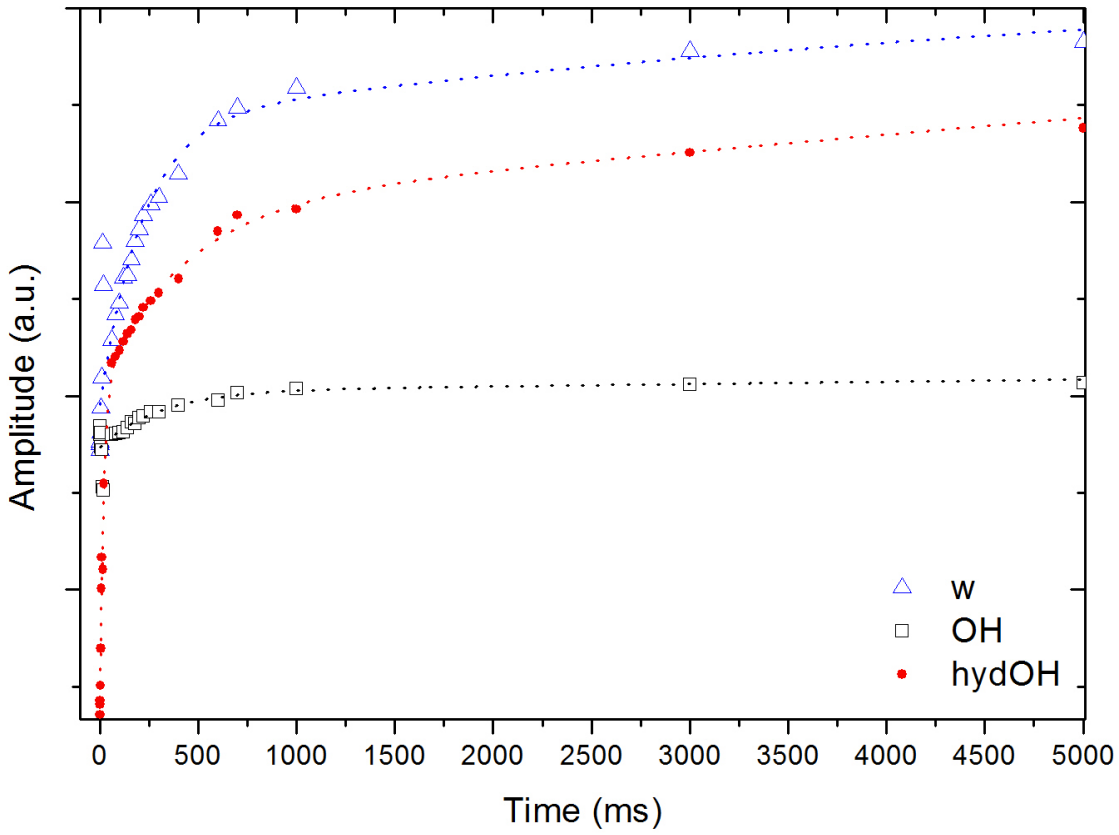

Figure 5.5: Evolution of different magnetization components in the M5min sample at 80 °C, as obtained in the selective inversion recovery experiment. Magnetization recovery time constants are as follow:

Spin Group	$(\lambda^+)^{-1}$	$(\lambda^0)^{-1}$	$(\lambda^-)^{-1}$
OH	-	(304±48) ms	(20±10) s
HydrOH	(19±2) ms	(424±148) ms	(30.8±19.6) s
Water	-	(218±66) ms	(6.6±4) s

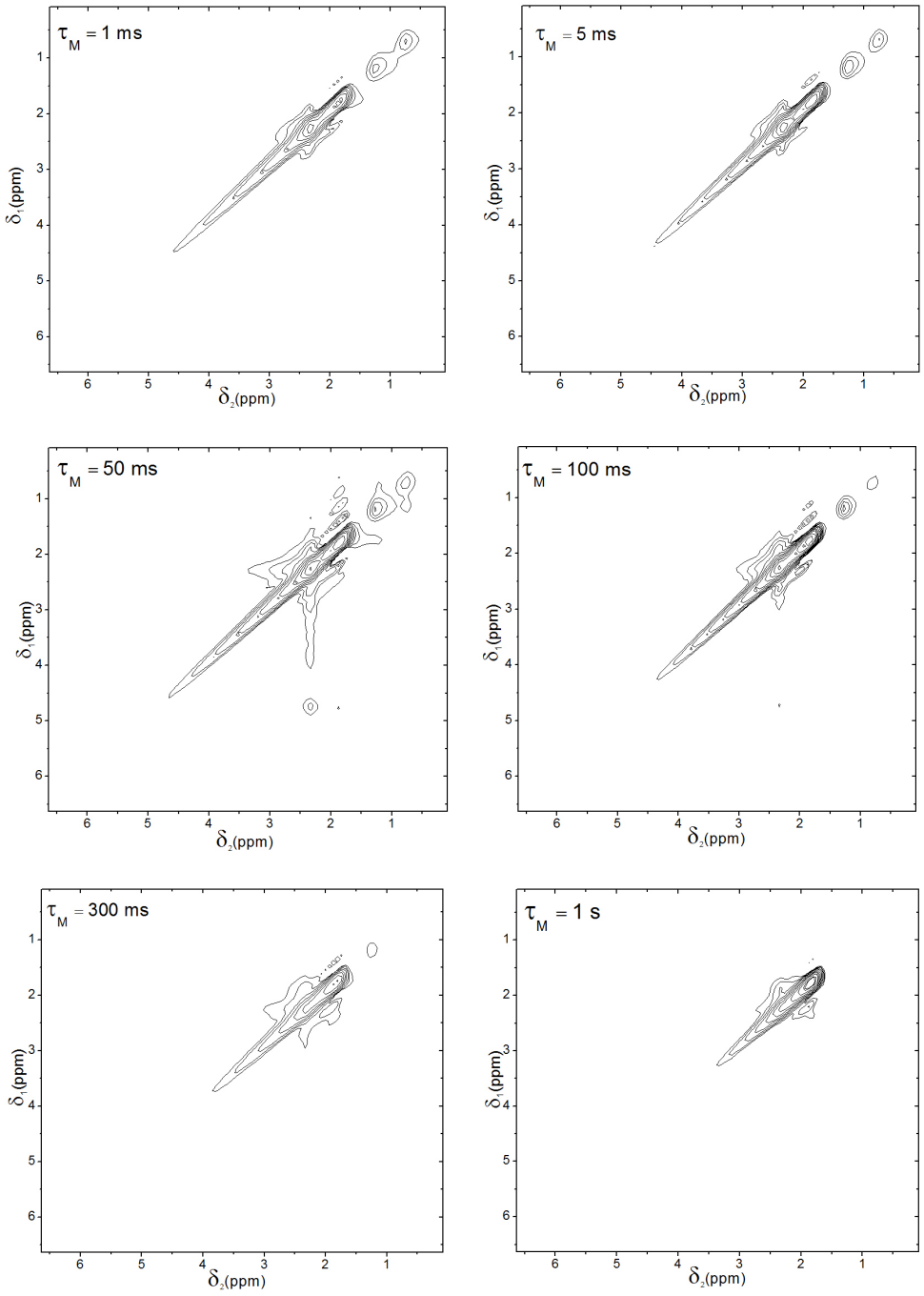

Figure 5.6: 2D exchange experiment in M20min sample at 20 °C. Lack of cross peaks that connect OH and water proton resonances, is an indication of slow exchange between these spin pools.

dipolar broadening not averaged by MAS and from a distribution of isotropic chemical shifts, which are not affected by MAS. For a Lorentzian, dipolar broadened line the 2D spectrum would be a square centred on the diagonal, with sides pulled towards the center of the square -the so called star-shaped pattern [23]. The OH peaks thus give rise to the observed star-like structure centered at about 2.5 ppm and elongated along the diagonal. Towards the bottom-left of the spectrum, the water peak is observable, which is spread along the diagonal due to a chemical shift distribution and to a much lesser degree in the direction perpendicular to the diagonal due to the width controlled by motional narrowing. Although at longer mixing time observation of slower exchange becomes possible, decrease of signal due to T_1 effects places limits on experiment duration. No distinct cross peaks between water proton resonances and surface OH proton resonances are visible. A slight broadening of the 2D spectrum is seen as τ_M is increased from 5 ms to 50 ms suggesting the presence of magnetization exchange between these spin pools on the time scale slower than 5 ms. As this is again considerably slower than the time defined by the inverse of the chemical shift differences, we take this result as supporting evidence for the conclusion that exchange is not the reason for the spectral features in question.

5.3 Dynamics model

Study of the temperature dependence of spectral line shape for the M20min sample MCM-41 sample gives more insight into the origin of the hydrated OH group proton resonance line. Figure 5.7 shows the spectral decompositions into three Lorentzian lines for two different temperatures. The spectrum on the top is for the M20min sample at 0 °C. The single OH group proton resonances at 1.7 ppm makes up 60 % of the total OH proton

signal. This implies that 40 % of surface OH group proton signal is chemically shifted by water, to 2.3 ppm. On the bottom the proton spectrum of the same sample at 80 °C shows that the hydrated OH group proton resonance line and the unaffected OH group proton resonance line have coalesced. Fitting three Lorentzian lines to this spectrum, while fixing the position of OH group proton peak to 1.9 ppm, as found from the data in the 60 °C experiment, gives that only 17 % of OH group protons are at their original chemical shift position and 83 % of OH protons contribute to the hydrated OH group peak at 1.9 ppm. This indicates that shifts of OH group proton resonances, from the original position in the dry sample, would be more effective when the number of modified sites is lower.

The above can be understood by considering the possible geometries of water attachment to surface OH groups. Figure 4.5 shows two hydrogen bond arrangements connecting water molecules to OH groups on the surface of MCM-41. [7] On the right hand side, the hydrogen of the surface OH group takes part in the hydrogen bond with the visiting water molecule, which changes the OH proton chemical shift position from 1.75 ppm to 5.5 ppm. In contrast, on the left hand side, a water molecule hydrogen takes part in the hydrogen bond which will change the water molecule hydrogen's proton resonance line position. As we increase moisture content of the sample, there are more water molecules, and the number of hydroxyl group protons with peak position shifted to 5.5 ppm, would increase. In addition, for a given moisture content the number of hydroxyl group protons being affected is also expected to depend on temperature. Such temperature influence will be explained below.

Consider a nano tube with some hydration sites on it's internal surface, containing water molecules much smaller in number than the number of OH groups. A water molecule visits a hydration site, where it makes a hydrogen bond to the surface OH group and after some

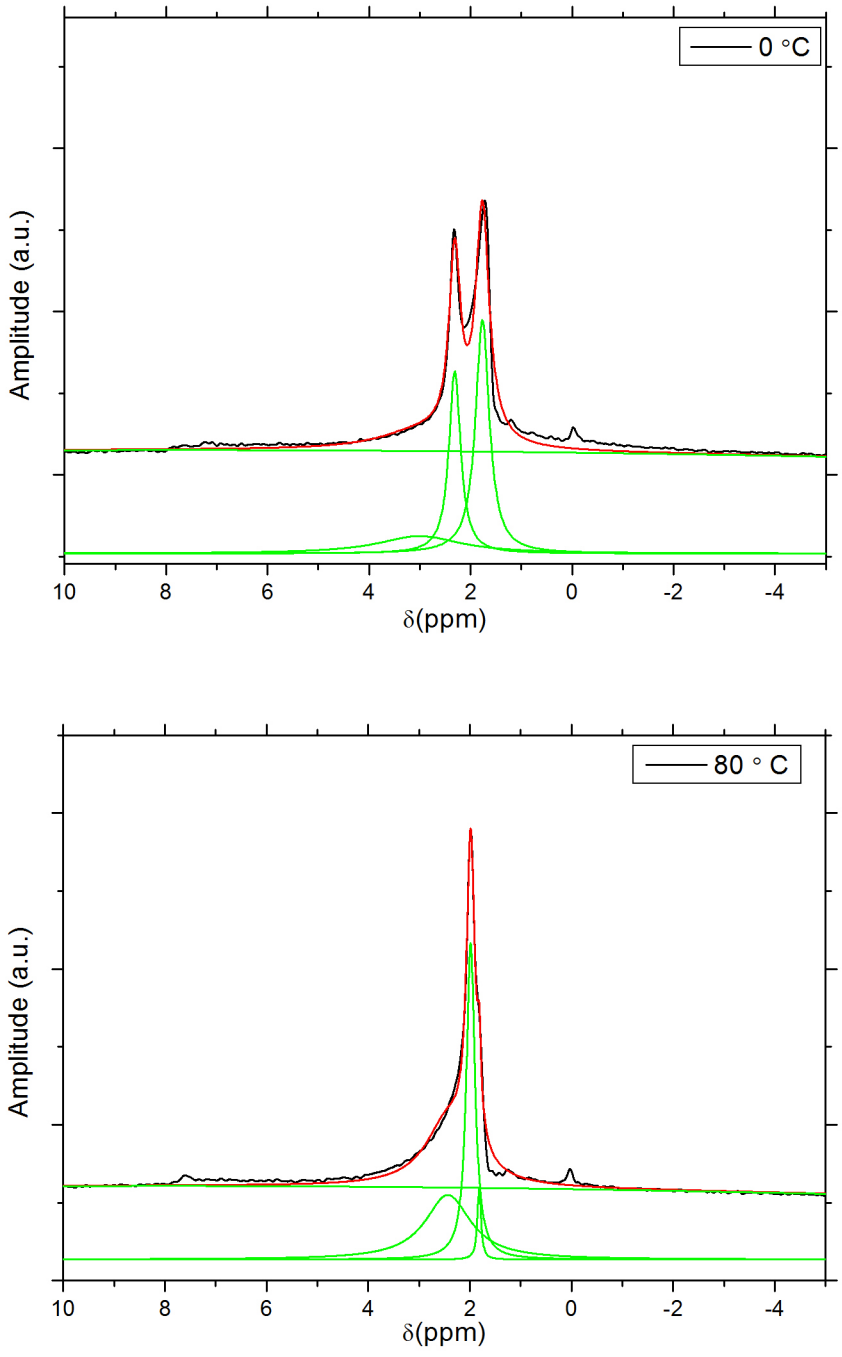

Figure 5.7: Decomposition of ^1HMAS signal of the M20min sample into three Lorentzian lines at 0 °C and 80 °C

time it will leave to visit another hydration site. If this water molecule can visit more than one hydroxyl group over the experimental time scale, the observed chemical shift position for the visited OH groups would be an average of chemical shifts of a visited/hydrated OH group proton and original OH group proton, weighted by the fraction of time the water molecule spent in each state. The water molecules are expected to perform random walks among the hydration sites. Neglecting the time of flight between OH groups, increasing the temperature will allow a water molecule to visit a larger number of hydration sites in the experimental time frame, although this will reduce the residence time at each OH group visited. This is exactly what has been observed in the temperature dependence experiment, Figure 5.7; i.e. with increasing temperature a larger number of OH group proton resonances have been modified (peak at δ_{hydOH} increases with temperature) while the shift away from δ_{OH} decreases. Decreasing temperature will have the reverse effect, Figure 5.3.

In order to quantify the above so that this model can be compared to experiment we consider the following simplified model. The fraction of time, f, that a hydration site is in a hydrated state is

$$f = \frac{\#\text{of water molecule}}{\#\text{of OH groups}} \tag{5.1}$$

Therefore the weighted average of chemical shifts (of visited OH group and of OH group not visited) becomes

$$\delta_{hydOH} = f\delta_{Havg} + (1-f)\delta_{1.75} \tag{5.2}$$

where δ_{Havg} is a weighted average of chemical shifts for a hydrated OH proton produced by the water molecule assuming the two hydration configurations shown in figure 4.5. Assume that the probabilities of the water molecule being in coordination (a) and (b) are p_a and

$(1 - p_a)$, respectively. Then

$$\delta_{Havg} = p_a\delta_{1.75} + (1 - p_a)\delta_{5.5} \tag{5.3}$$

and

$$\delta_{hydOH} = f(p_a\delta_{1.75} + (1 - p_a)\delta_{5.5}) + (1 - f)\delta_{1.75} \tag{5.4}$$

Thus, the effective chemical shift produced by the visiting water molecule is linearly dependent on the fractional residence time f.

In addition, decreasing the fractional residence time for a water molecule, will linearly increase the number of OH group sites accessed (neglecting flight time). Therefore, if this averaging of chemical shift positions is the cause of OH group proton chemical shift changes, the number of modified OH group protons should linearly relate to the residence time or the average OH group proton chemical shift position. As already mentioned we can control the number OH group sites accessed by water by changing temperature. Figure 5.8 shows that the number of modified OH group protons have a linear relationship with the chemical shift difference from the original OH group proton chemical shift position. This observation supports the proposed model for the origin and behaviour with temperature of the hydrated OH group proton peak.

Further confirmation of the above model comes from a calculation of average chemical shift positions for each spin group using this model. In Equation (5.4), with substitution of δ_{hydOH} and replacing f with amplitude of water peak/amplitude of OH peak, p_a is found to be 75 % at room temperature. Using this calculated p_a in the following equation will

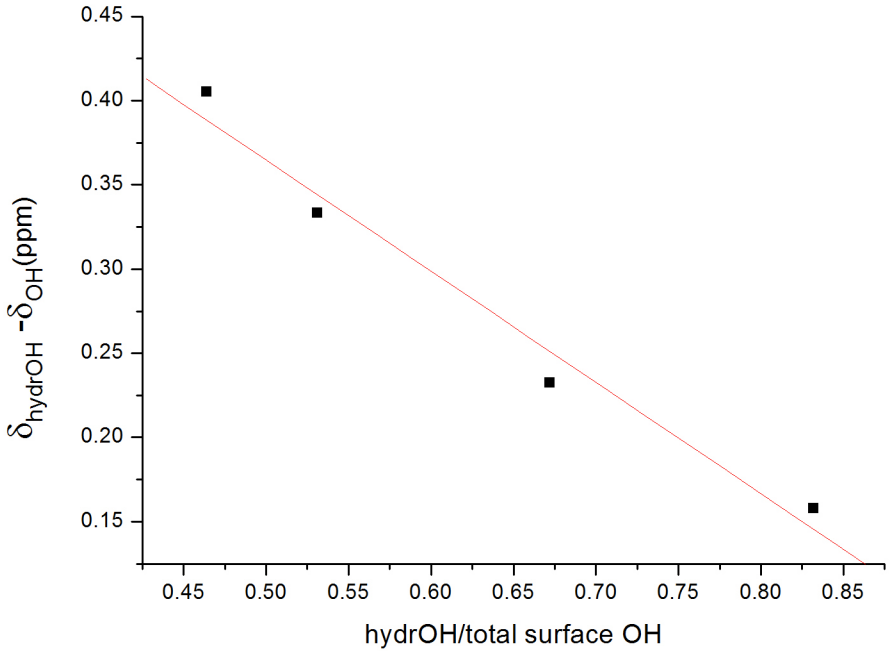

Figure 5.8: Chemical shift change ($\delta_{hydrOH} - \delta_{OH}$) versus number of hydrated OH groups in the M20min sample. The different chemical shift changes are obtained from the temperature run, Figure 5.3.

give an estimate of the average chemical shift for water protons

$$\delta_w = p_a \delta_{(5.5+1.5)/2} + (1 - p_a)\delta_{1.5} \tag{5.5}$$

This gives $\delta_w = 3$ ppm, in complete agreement with the observed data, Figure 5.2 .

Chapter 6

Conclusion

Spectral features of hydrated MCM-41 proton resonances have been studied using MAS at 500 MHz as well as low frequency time domain relaxation experiment. In the literature, chemical exchange between surface OH protons and water protons is assumed to be the main cause for changes in proton resonance line shape as dry MCM-41 is hydrated.[7] Through exchange model simulations it has been shown here that for appreciable changes in proton resonance lines to be realized upon hydration, a fast exchange rate of the order of 1000 s^{-1} or higher, is needed. However, using SH inversion recovery experiments, the highest exchange rate found in a hydrated sample was only 300 s^{-1}. These observation indicate that processes other than magnetization exchange must be involved in explaining spectral line shapes in hydrated samples of MCM-41. The particular importance of this result is that interpretation of proton spectra in this material, based on the assumption that the spectral line chemical shift is produced by magnetization exchange, is not valid and the origin of chemical shifts of spectral lines in MCM-41 should be studied more carefully.

One of the more significant problems in this type of study is the definitive assignment

of resonance lines to proton groups in the material. This was addressed by using very low hydration samples (400dry). This, combined with experiments at different hydration levels, allowed us to identify the water proton resonance line, thus enabling the knowledge-based interpretation of the very low hydration spectra. This, in turn, has led to the elucidation of details pertaining to the interaction between water (protons) and surface (protons).

Temperature dependent experiments prompted us to address the problem of a small number of water molecules shifting the proton resonance of a much larger number of OH groups. It was concluded that such shift was produced by an averaging of the chemical shift of non-hydrated OH protons and hydrated OH protons, weighted by the fractional residence time.

The chemical shift position of each proton group (water, OH and hydrated OH) has been calculated by averaging over the different chemical shift positions available for the different hydration configurations on OH groups. The calculated values were in agreement with the observed data.

Based on the present results we have proposed the the following mechanism produces the observed chemical shift changes in the OH and water proton resonances as MCM-41 being hydrated. Each water molecule will visit a certain number of hydration sites, each for a limited residence time, while forming a hydrogen bond with the site. The residence time of the water molecule at a surface OH site depends on temperature. The combination of different hydration coordination defines the chemical shift positions of the resulting resonance lines for water and OH groups. Adding more water increases the number of hydrated sites (as well as the number of times that each site could be visited), which will define the chemical shift position of the hydrated OH peak and water peak at different hydration levels. Thus, rather than resulting from chemical exchange, the observed changes

in chemical shifts are produced by specific details of water molecule dynamics on the MCM-41 pore surface.

Recommendations

Water is expected to undergo anisotropic motion at the OH group hydration sites. Earlier NMR work in MCM-41 has suggested that such motion can be studied through ^2H NMR experiments. Specifically, preferred direction of the water molecule (and its deuterons) in the two hydrogen-bonding coordination, may result in the splitting of the ^2H resonance lines. Thus, ^2H spectral experiments in deuterated MCM-41 samples, at very low hydrations, are recommended. The proposed model of fractions of each hydration configuration found in the present study could then be compared to results predicted from the modelling of the ^2H resonance line structures.

Exchange measurements on deuterated MCM-41 samples is expected to be very useful because relaxation times in the deuteron case are much shorter than for protons, which would allow us to observe exchange of magnetization on different time scales.

In connection with the initial problem of this work, monitoring changes of the water proton peak and OH proton peaks with hydration, gradually being increased from 0 % moisture content to n = 1, could give further insight into resonance line shape origins at higher hydrations.

Bibliography

[1] Bronnimann, C. E., Zeigler, R. C., and Maciel, G. E. *J. Am. Chem. Soc.* **110**, 2023–2026 (1988). 1

[2] Overloop, K. and Gerven, L. V. *J. Magn. Reson. A* **101**, 147–156 (1993). 2

[3] Zhao, X., Lu, G., Whittaker, A., Millar, G., and Zhu, H. *J. Phys. Chem. B* **101**, 6525 (1997). 2, 27

[4] Hwang, L.-P., Hwang, D. W., Sinha, A. K., Yu, T.-Y., and Cheng, C.-Y. *Magn. Reson. Imaging* **19 (3-4)**, 275–276 (2001). 2

[5] Hwang, D. W., Sinha, A. K., Cheng, C.-Y., Yu, T.-Y., and Hwang, L.-P. *J. Phys. Chem. B* **105**, 5713–5721 (2001). 2

[6] Pizzanelli, S., Kababya, S., Frydman, V., Landau, M., and Vega, S. *J. Phys. Chem. B* **109**, 8029–8039 (2005). 2

[7] Grunberg, B., Emmler, T., Gedat, E., Shenderovich, I., Findenegg, H., Limbach, H., and Buntkowsky, G. *Chem. Eur. J.* **10**, 5689 (2004). 2, 29, 47, 54, 60

[8] Trebosc, J., Wiench, J., Huh, S., Lin, V., and Pruski, M. *J. Am. Chem. Soc.* **359**, 127 (2005). 3

[9] Hassan, J., Reardon, E., and Peemoeller, H. *Micropor. Mesopor. Mater.* **122**, 121–127 (2009). 3, 27, 41

[10] Mehring, M. *Principles of High Resolution NMR in Solids.* Springer-Verlag, (1983). 7

[11] Hassan, J. *NMR study of exchange and hydration site identification in MCM-41.* PhD thesis, University of Waterloo, (2006). 8, 21

[12] Levitt, M. H. *Spin Dynamics, Basics of Nuclear Magnetic Resonance.* John Wiley & Sons, (2001). 9

[13] Slichter, C. *Principles of Magnetic Resonance.* Springer-Verlag, (1980). 5, 9, 11

[14] Oleskevich, D. A., Ghahramany, N., Weglarz, W. P., and Peemoeller, H. *J. Magn. Reson.* **113**, 1–8 (1996). 16, 39

[15] Liang, J. Master's thesis, University of Waterloo, (2005). 17, 27, 29, 37

[16] Weglarz, W. Technical report, PDF in Waterloo NMR laboratory, (1995). 18

[17] Mansour, F., Dimeo, R. M., and Peemoeller, H. *Phys. Rev. B* **66**, 041307 (2002). 20, 21

[18] Kresge, C., Leonowicz, M., Roth, W., Vartuli, J., and Beck, J. *Nature* **359**, 710–712 (1992). 20

[19] Resing, H. A. *J. Phys. Chem.* **80** (1976). 32

[20] Lynch, L. J. and Marsden, K. H. *J. Colloid Interface Sci.* **42**, 209–213 (1973). 32

[21] Edzes, H. T. and Samulski, E. T. *J. Magn. Reson.* **31**, 207–229 (1978). 35

[22] Lattanzio, P., Marshall, K., Damyanovich, A., and Peemoeller, H. *Magn. Reson. Med.* **44**, 840–851 (2000). 36

[23] Ernst, R. R., Bodenhausen, G., and Wokaun, A. *Principles of nuclear magnetic resonance in one and two dimensions*. Oxford University Press, (1987). 53